frontiers | Frontiers in Earth Science

TYPE Original Research
PUBLISHED 24 January 2023
DOI 10.3389/feart.2023.1062956

OPEN ACCESS

EDITED BY
Jing-Jing Zhu,
Institute of Geochemistry (CAS), China

REVIEWED BY
Teng Deng,
East China University of Technology, China
Rui Wang,
China University of Geosciences, China

*CORRESPONDENCE
Lingli Guo,
guolingli@ouc.edu.cn
Junjiang Zhu,
zhujunjiang@ouc.edu.cn

SPECIALTY SECTION
This article was submitted to Geochemistry, a section of the journal Frontiers in Earth Science

RECEIVED 06 October 2022
ACCEPTED 09 January 2023
PUBLISHED 24 January 2023

CITATION
Hao Y, Guo L, Feng Y, Zhang H, Somerville I, Li S and Zhu J (2023), Petrogenesis and tectonic settings of epithermal mineralization-related granites in the Xinchenggou area, NE China. *Front. Earth Sci.* 11:1062956. doi: 10.3389/feart.2023.1062956

Petrogenesis and tectonic settings of epithermal mineralization-related granites in the Xinchenggou area, NE China

Yi Hao[1], Lingli Guo[2]*, Yingming Feng[1], Hao Zhang[1], Ian Somerville[3], Sanzhong Li[2] and Junjiang Zhu[2]*

[1]The First Prospecting Team of Shandong Coal Geology Bureau, Qingdao, China, [2]Key Lab of Submarine Geosciences and Prospecting Techniques, Ministry of Education, and College of Marine Geosciences, Ocean University of China, Qingdao, China, [3]UCD School of Earth Sciences, University College Dublin, Dublin, Ireland

The Xinchenggou area is located in the northeast part of the eastern segment of the Xingmeng orogenic belt (EXOB), NE China and has been demonstrated to be a promising exploration target for epithermal deposits. Although previous studies have shown that syenogranite and monzogranite occurring in the Xinchenggou area are promising in forming epithermal mineralization, the petrogenesis and geodynamic settings in which these granites were emplaced are still unclear. To address these problems, in this study detailed whole-rock major and trace element analyses for these granites were conducted. Combined with previously published data, we show that both syenogranite and monzogranite in the Xinchenggou area are high-K calc-alkaline and peraluminous with high SiO_2. Their rare earth element concentrations are low ($\Sigma REE = 72.35 \times 10^{-6}–217.64 \times 10^{-6}$) and show obvious differentiation between LREE and HREE (La_N/Yb_N=2.74–11.37), with apparent Eu negative anomalies (δEu = 0.14–0.83) and indistinctive Ce anomalies (δCe = 0.96–1.11). Combined with petrographical observations, it is suggested that both syenogranite and monzogranite are (slightly fractionated) I-type granite. Nb/Ta ratios of syenogranite and monzogranite range from 6.18 to 26.33, indicating that the granitic magma was derived from the upper mantle or the lower crust. Both syenogranite and monzogranite were emplaced in a continental arc setting, which was related to the subduction of the Paleo-Pacific Plate beneath the Eurasian Plate during the Late Triassic to Early Jurassic.

KEYWORDS

Xinchenggou area, active continental margin, granite, geochemistry, tectonics, metallogenic potential

1 Introduction

The eastern segment of the Xingmeng orogenic belt (EXOB), NE China, is located in the superposition of the Paleo-Asian and Mongolia-Okhotsk oceanic and Paleo-Pacific tectonic metallogenic domains (Wang YB. et al., 2016; Zhong et al., 2017; Wang et al., 2021; Tang et al., 2023). This region is one of the most important polymetallic-ore regions globally and is characterized by large reserves of Ag, Pb-Zn, Cu, Mo, Sn, and Au (Wang et al., 2021; Zhang et al., 2022).

In the past decade, extensive exploration work in this area has resulted in the discovery of several large and super-large deposits and numerous small deposits (Zhang et al., 2010b; Gao et al., 2017; Deng et al., 2021; Jiang et al., 2022). The formation of the deposits in the EXOB

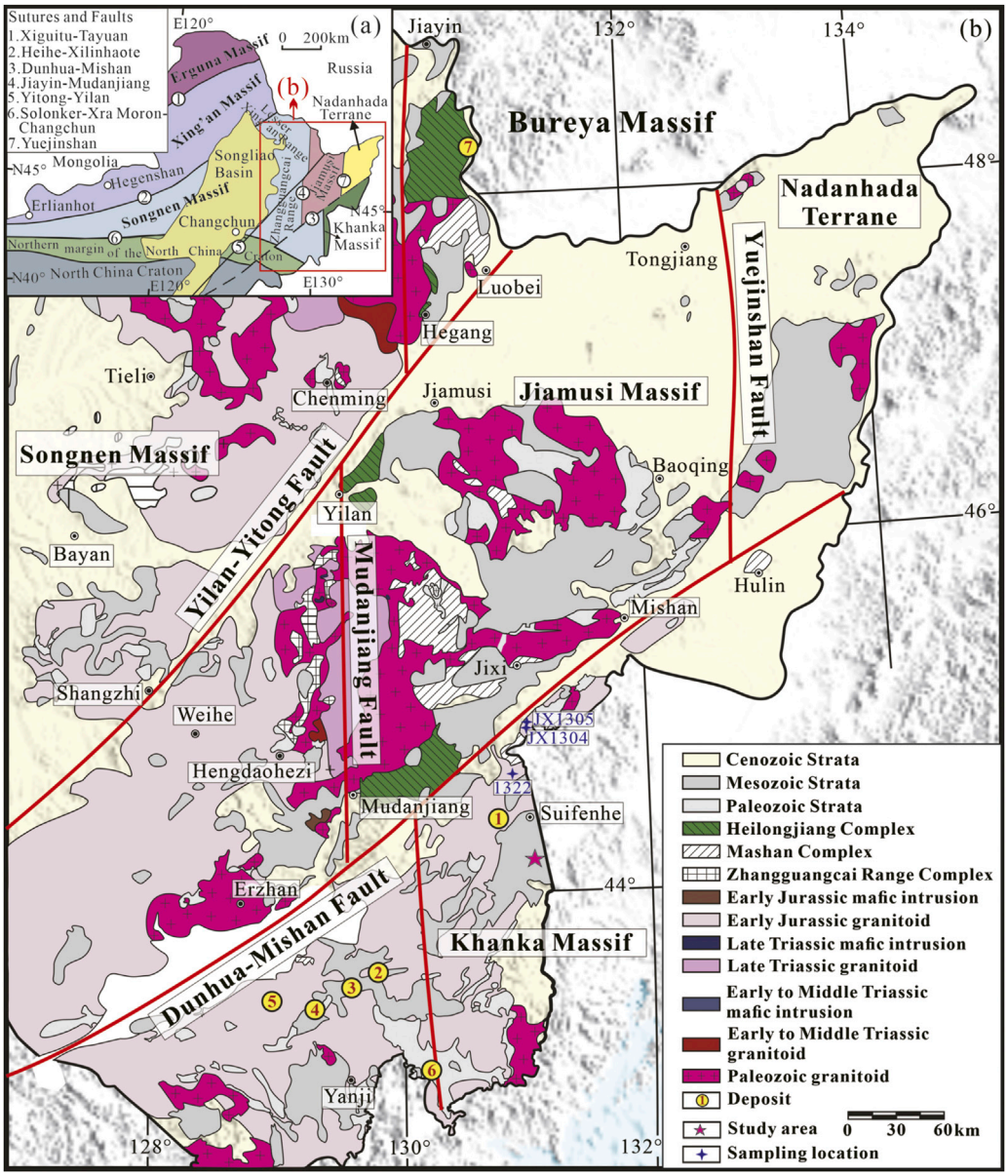

FIGURE 1
Tectonic sketch map of NE China **(A)** (modified from Xu et al., 2019); Polymetallic deposits in the Xinchenggou area **(B)** (modified from Zhang et al., 2008; Long et al., 2020).

has been demonstrated to be related to Mesozoic magmatic-hydrothermal activity, and the mineralization types primarily include porphyry, skarn, hydrothermal veins and epithermal deposits (Wang et al., 2021). Mineral exploration is still ongoing in this area and the potential for more discoveries exists. The Xinchenggou area is located in the Heilongjiang Province, NE China and belongs to the northeast part of the EXOB. This area is characterized by occurrences of many Mesozoic granitoids. A previous geological survey has shown that the Xinchenggou area is a promising exploration target for porphyry-epithermal deposits (Hao and Wang 2017). This is further demonstrated by discoveries of more than five porphyry-epithermal deposits in its adjacent area. Based on a detailed geophysical survey, Hao and Wang (2017) have also pointed out that the granitoids in the Xinchenggou area are fertile to form epithermal mineralization. However, many aspects of the granitoids in this area are still unclear, including their petrogenesis and geological settings. This hinders a better understanding of magmatic-hydrothermal activities and geodynamic settings in the Xinchenggou area. Thus, in this work, based on a detailed field survey, we conduct new major and trace element analyses on the ore-related syenogranite and monzogranite from the Xinchenggou area and a new geodynamic model is proposed. This, combined with the published geophysical and geochemical survey data, helps to better constrain the petrogenesis of ore-related granitoids and guide further mineral exploration in this area.

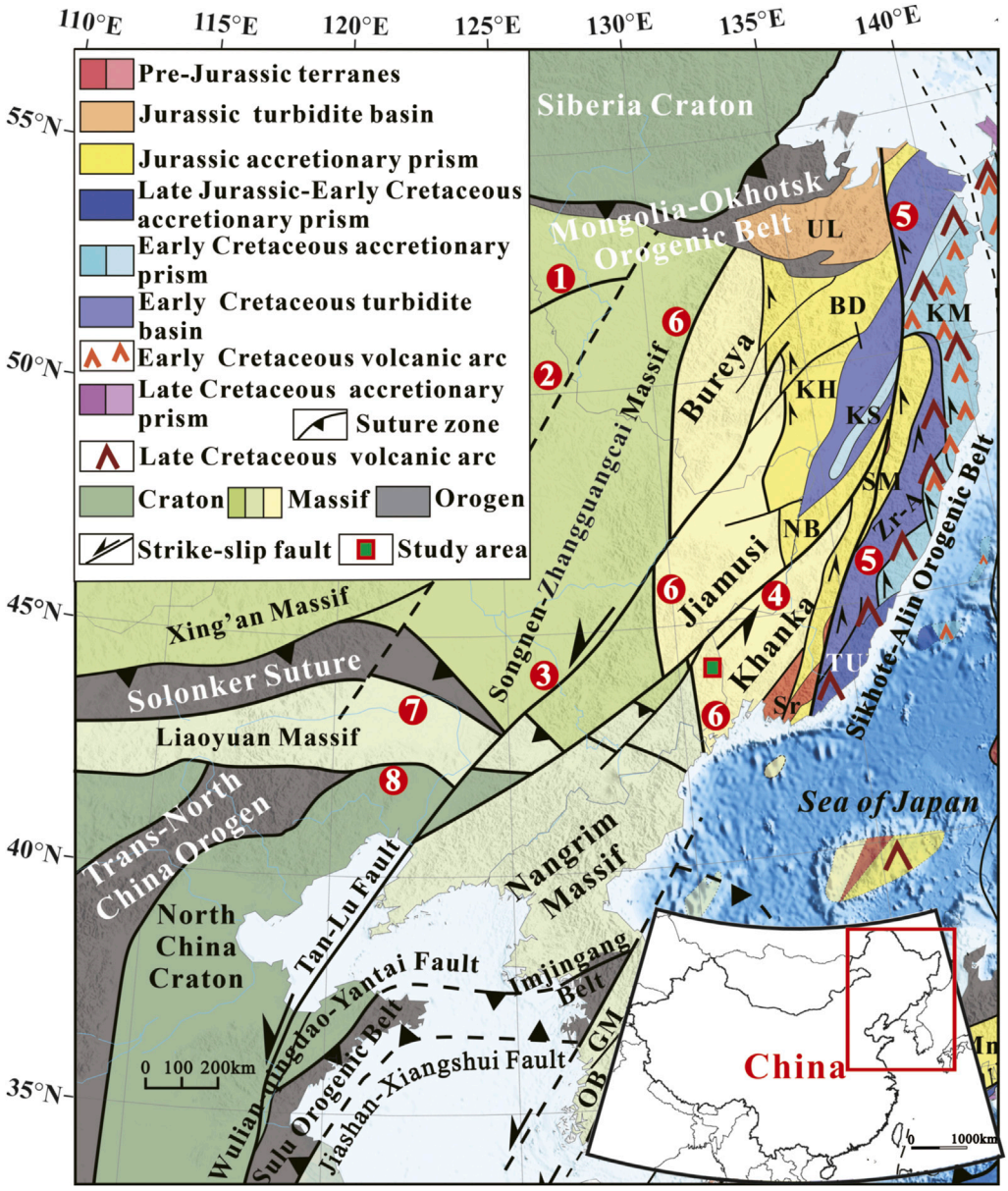

FIGURE 2
Simplified tectonic units of NE China (modified from Liu et al., 2021; Lan et al., 2022). 1-Xinlin-Xiguitu Fault; 2-Hegenshan-Heihe Fault; 3-Yilan-Yitong Fault; 4-Dunhua-Mishan Fault; 5-Central Sikhote-Alin Fault; 6-Jiayin-Mudanjiang Fault; 7-Solonker-Xar Moron-Changchun-Yanji Fault; 8-Northern margin fault zone of North China; BD-Badzhal; GM-Gyeonggi Massif; KH-Khabarovsk; KM-Kema; KS-Kiselevka-Manoma; NB-Nadanhada-Bikin; OB-Okcheon Belt; SM-Samarka; Sr- Sergeevka; TU-Taukhe; UL-Ul'ban; Zr-A-Zhuravlevka-Amur.

2 Geological background

2.1 Regional geology

As already mentioned, the EXOB is located in a region with a complicated overprinting and interaction of the Palaeozoic Palaeo-Asian tectonic–metallogenic domain and the Mesozoic Western Pacific margin tectonic–metallogenic domain (Figure 1A). The tectonic evolution of the EXOB has been especially studied in many studies, which we summarize here. The EXOB has undergone two stages of tectonic evolution in different tectonic settings (Wang YB. et al., 2016). In the Paleozoic, tectonism and magmatism were controlled by the evolution of the Paleo-Asian Ocean between the Siberia and the North China cratons (Wang and Mo, 1995). The EXOB was developed in this stage, accompanied by the amalgamation of several microcontinental blocks in NE China (Zeng et al., 2012; Ouyang et al., 2013): the Erguna block in the northwest, the Xing'an and Songliao blocks in the centre, the Liaoyuan block in the southeast and the Jiamusi-Khanka block in the northeast. Final closure of the Paleo-Asian Ocean marked by suturing between the Songliao block and the Liaoyuan block is believed to have taken place along the Solonker-Xar Moron-Changchun suture zone at ca. 250 Ma (Xiao et al., 2003; Wu et al., 2011; Ouyang et al., 2013). However, other studies suggest that this event may have occurred at ca. 230 Ma (Zhou

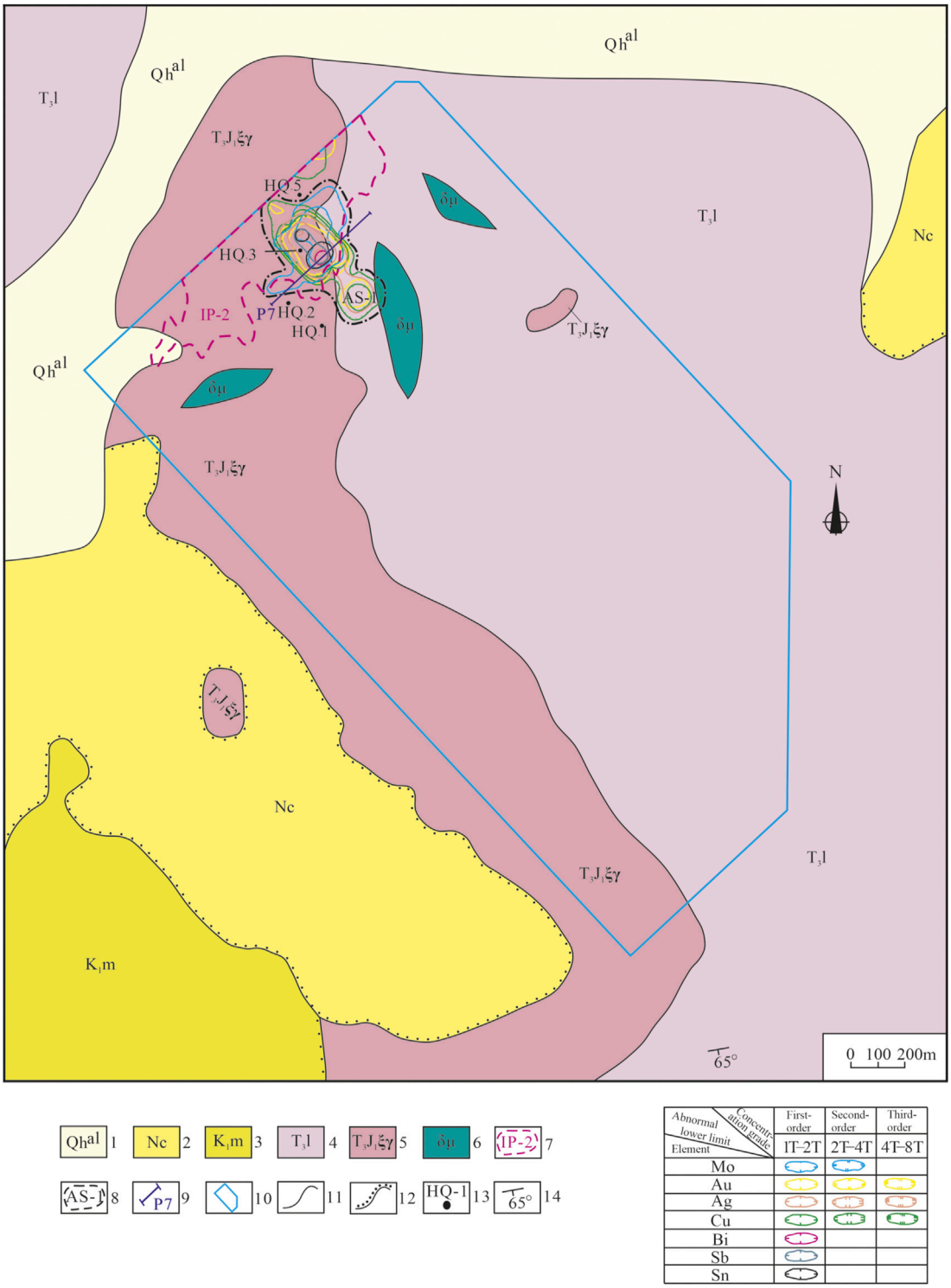

FIGURE 3
Simplified geological map of the Xinchenggou area, Dongning County. 1-Holocene Epoch Quaternary System; 2-Miocene-Pliocene Chuandishan Formation; 3-Early Cretaceous Muleng Formation; 4-Late Triassic Luoquanzhan Formation; 5-Late Triassic-Early Jurassic syenogranite; 6-Dioritic porphyrite; 7-Anomaly of IP Mid gradient and its number; 8-Anomaly of soil geochemical survey and its number; 9-Profile of soil geochemical survey and its number; 10-Mine field border; 11-Geological boundary; 12-Angular unconformity boundary; 13-Sampling position; 14-Attitude.

and Wilde, 2013). Since the Early Jurassic, the tectonic framework of northeastern China has been dominated by the subduction of the Paleo-Pacific oceanic plate in the east (Wu et al., 2011; Zeng et al., 2012; Xu et al., 2013a; Zeng et al., 2013), which induced extensive magmatic activities throughout the EXOB (Wu et al., 2011). The deposits in the study area mainly belong to the Yanshanian intermediate-acid magmatism Au, Ag, Cu, Pb, Zn (Mo) metallogenic series, which is controlled by structure, rock strain

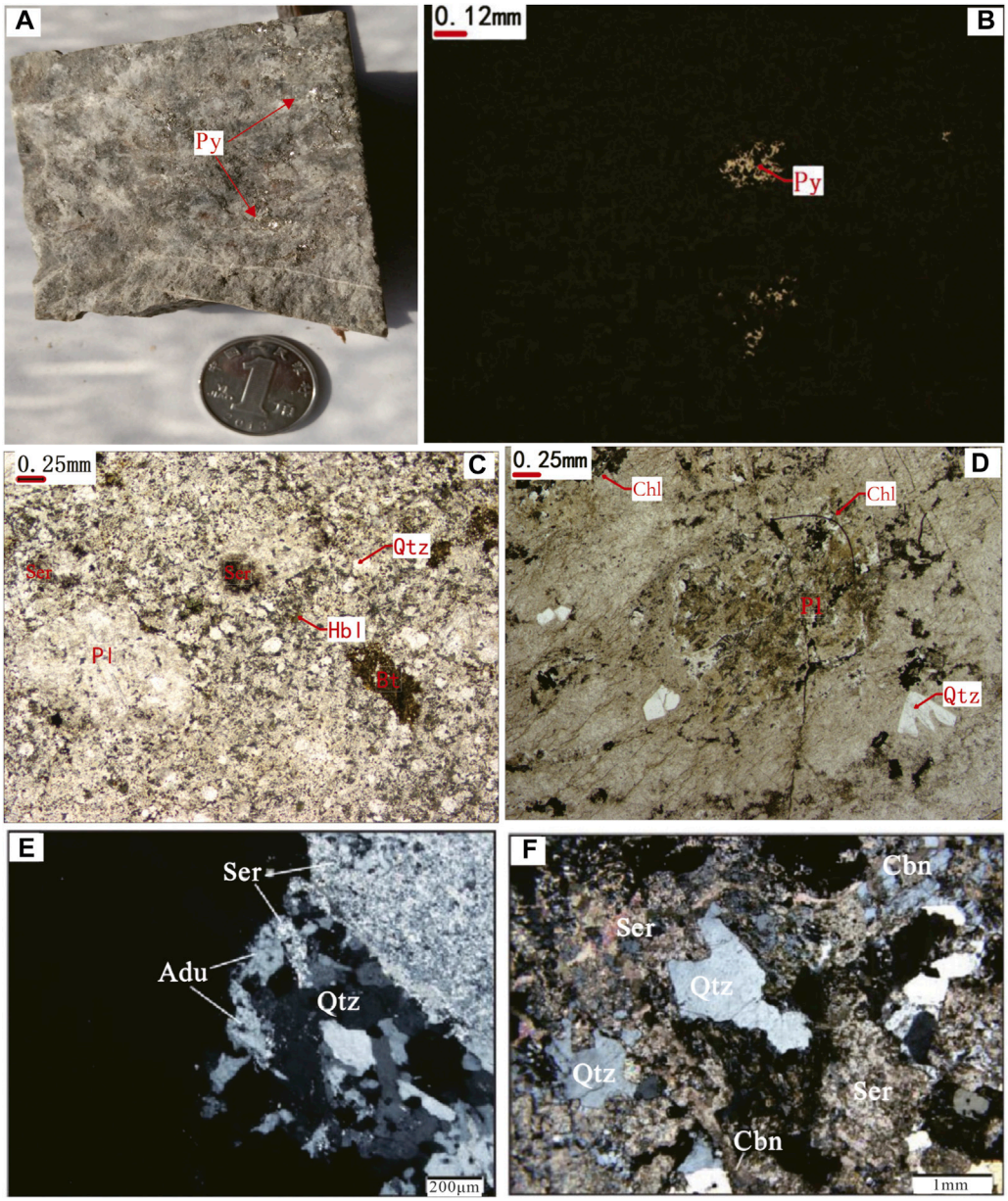

FIGURE 4
Mineralized, altered and microscopic characteristics of surrounding rocks in the study area (E, F modified from Li, 2021). **(A)** Hand specimen of pyritic dacite; **(B)** Microscopic characteristics of pyrite in pyrized dacite; **(C)** Microscopic characteristics of sericite in syenogranite; **(D)** Microscopic characteristics of chlorite in syenogranite; **(E)** Microscopic characteristics of feldspar and sericite in pyritic sericite; **(F)** Microscopic characteristics of sericite and carbonation in granodiorite. Abbreviations: Py, Pyrite; Ser, Sericite; Hbl, Hornblende; Chl, Chlorite; Adu, Adularia; Cbn, Carbonate mineral; Bt, Biotite; Pl, Plagioclase; Qtz, Quartz.

and subvolcanic porphyry. The complex geological evolution has resulted in intense magmatism as well as extensive precious and non-ferrous metal mineralization in this area, especially epithermal gold mineralization (Ge et al., 2007; Zeng et al., 2011; Zeng et al., 2012; Ouyang et al., 2013).

A lot of gold deposits (Figure 1B), including epithermal, metamorphic hydrothermal, magmatic hydrothermal, orogenic, porphyry and skarn gold deposits, have been discovered in recent years in Heilongjiang province. In the porphyry-epithermal metallogenic system, porphyry deposits are enriched in intrusive rocks, and epithermal deposits cover the top of intrusions, and the metallogenic age of the latter is generally 10~20 Ma later than the former (Wang et al., 2012). The low-density gas fluid in the porphyry metallogenic domain can carry ore-forming metals to migrate to the epithermal metallogenic domain, and gradually transform into low-temperature and low-salinity liquid fluid through gas phase contraction (Ni et al., 2020). The porphyry - epithermal deposit in Xinchenggou area is mainly Jinchang copper - gold deposit. In Jinchang deposit, there is a transformation from veinlet-impregnated ore body to cryptoexplosive breccia ore body, that is the transformation from porphyry gold-copper deposit (No.18 copper-gold deposit) to epithermal high-sulfide deposit

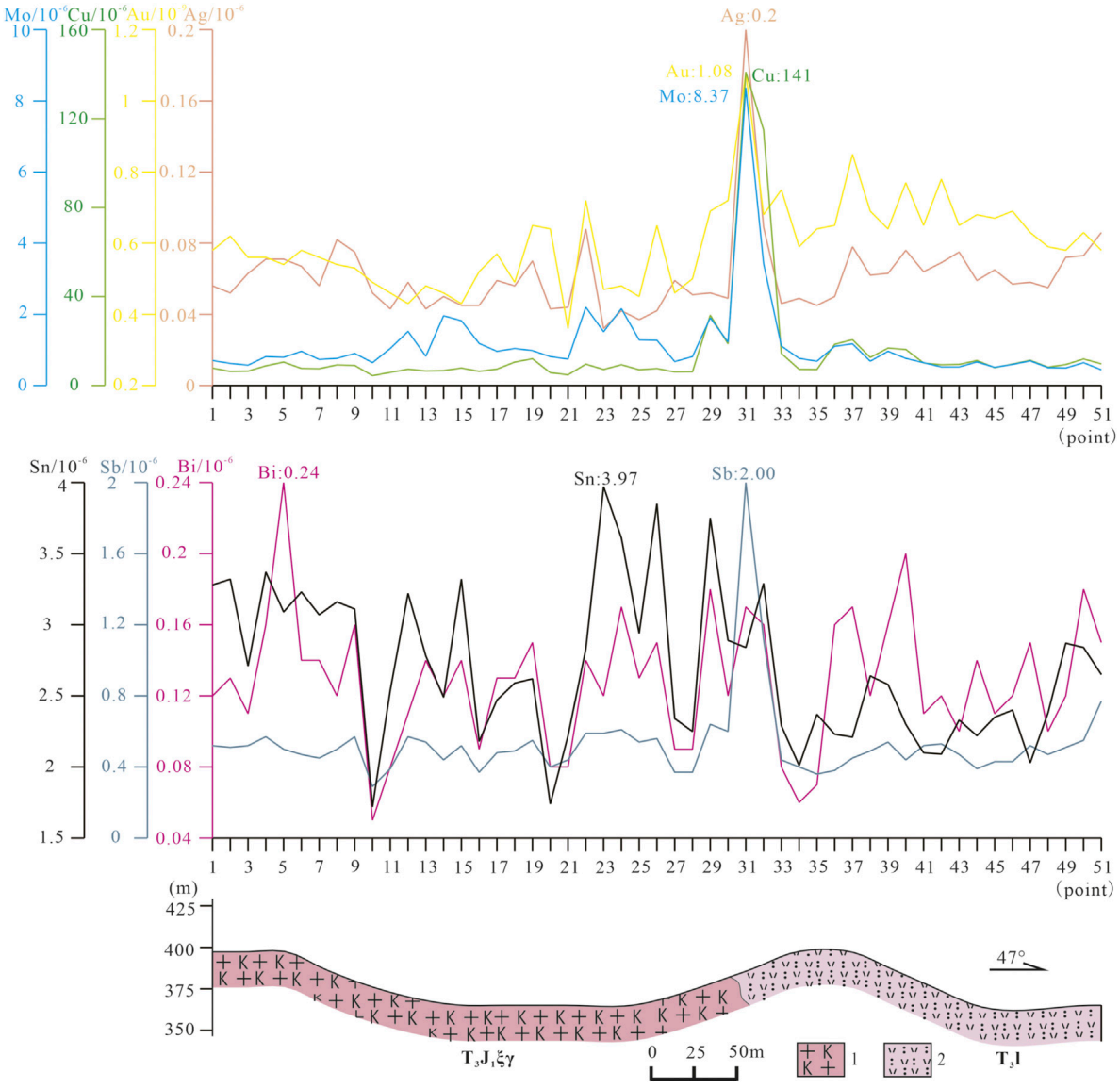

FIGURE 5
Integrated section of Line P7 in the Xinchenggou area, Dongning County. 1-Late Triassic-Early Jurassic syenogranite; 2-Late Triassic Luoquanzhan Formation.

(No.1 breccia gold deposit) (Wu, 2018). Among these gold deposits, epithermal gold deposits (including Wulaga, Dong'an, Sandaowanzi and Sipingshan epithermal gold deposits; Wang YB. et al., 2016) account for more than 60% of present estimates of the gold resource in Heilongjiang province and these deposits are believed to be associated with Early Cretaceous volcanic and subvolcanic intrusions (Wang et al., 2016a; and references therein). In the past, there have been many studies on single deposit, but few studies on the distribution characteristics and metallogenic rules of the whole metallogenic zone.

2.2 Geology of the Xinchenggou area

The Xingchenggou area tectonically belongs to the Khanka block in the EXOB (Figure 1; Figure 2). It is adjacent to the Songnen-Zhangguangcai Range along the Jiayin-Mudanjiang Fault to the west, the Sikhote-Alin Orogenic Belt along the Central Sikhote-Alin Fault to the east, and the Jiamusi Terrain along the Dunhua-Mishan Fault to the north. The Khanka Terrain mainly comprises the Precambrian metamorphic complex, early Paleozoic -Cenozoic sedimentary cover, Mesozoic granite and Late-Middle Permian-Late Triassic igneous rock (Wang F. et al., 2016). The Mesozoic and Cenozoic strata in the study area belong to marginal-Pacific strata, including the Late Triassic Luoquanzhan Formation (T_3l), Early Cretaceous Muling Formation (K_1m), and Miocene-Pliocene Chuandishan Formation (N*c*) (Figure 3). In terms of the rock assemblages, most of them are tuff, sandstone and basalt. Magmatic activities in the area mainly occurred during the Late Triassic-Early Jurassic. Petrographically, most of them are medium-coarse-grained syenogranite, and to a lesser extent diorite porphyry dykes. The major deformation structure are faults and there are no noticeable folds. The faults are dominated by the NE-extending, high-angle thrust fault structure which was formed before the Late

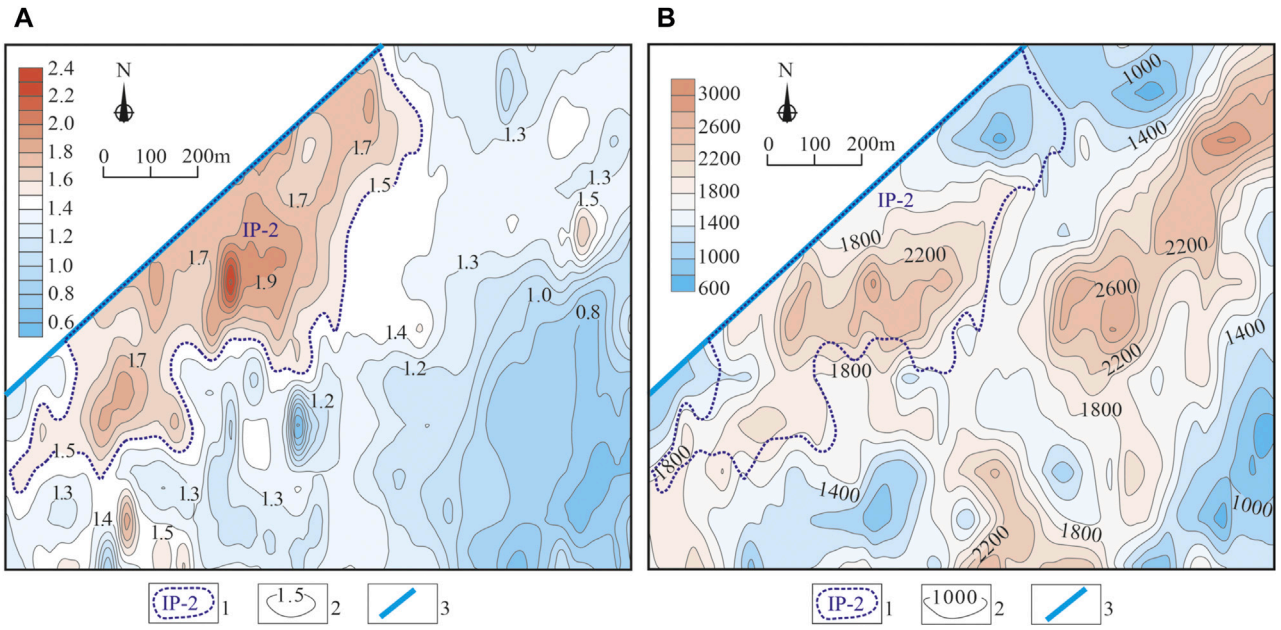

FIGURE 6
Plan-view contour of IP Mid gradient polarizability(η_s) **(A)** and IP Mid gradient apparent resistivity(ρ_s) **(B)** of Xinchenggou area, Dongning County. 1-Anomaly of IP Mid gradient and its number; 2-Anomaly contour and value; 3-Mine field border.

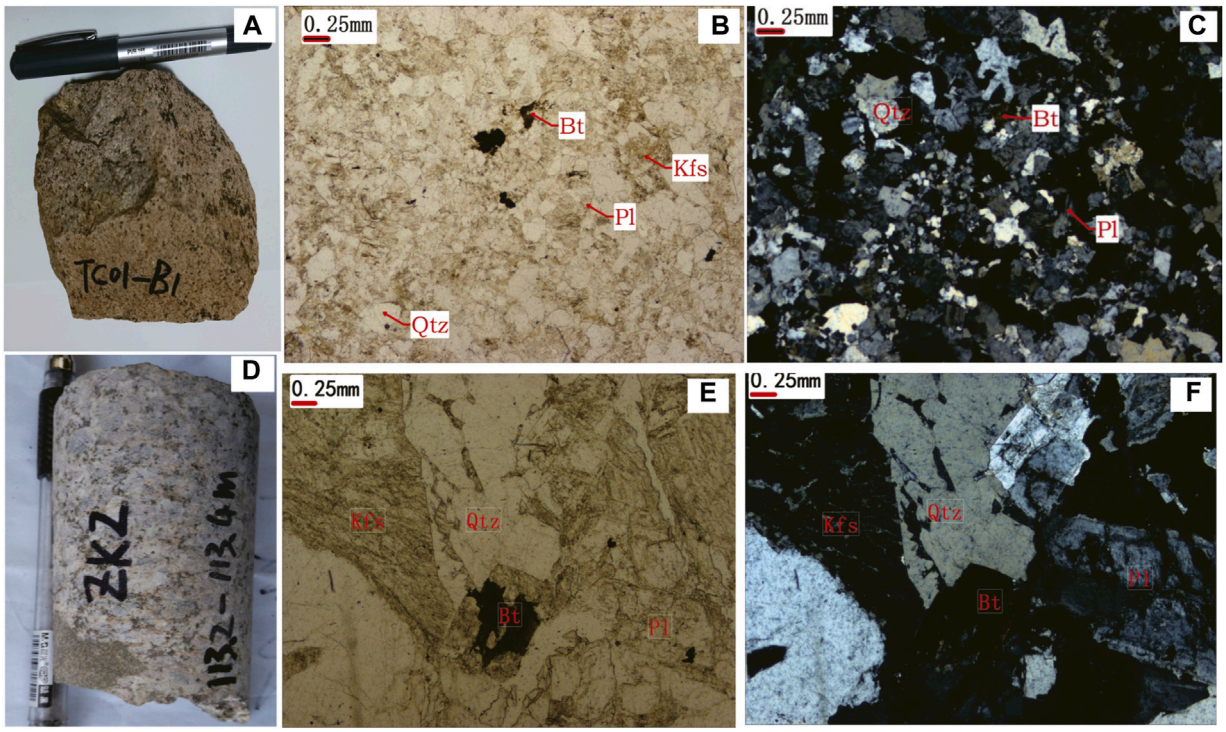

FIGURE 7
Representative hand sample and photomicrographs for the granitic intrusions in the Xinchenggou area, Dongning County. **(A)** syenogranite; **(B)** syenogranite inplane-polarized light; **(C)** syenogranite in cross-polarized light; **(D)** monzogranite; **(E)** monzogranite in plane-polarized light; **(F)** monzogranite in cross-polarized light. Abbreviations: Kfs, K-feldspar; Bt, Biotite; Pl, Plagioclase; Qtz, Quartz.

Triassic. The emplacement of the Mesozoic magmatic rocks is controlled mainly by these faults. It also can be observed that the early Paleozoic strata and granitic plutons are locally cut by faults.

The relationship between the Khanka Terrain and the Jiamusi Terrain is still debated. Based on zircon dating and whole-rock geochemical results for Permian volcanic rocks at the eastern and

TABLE 1 Petrographic characteristics of syenogranite and monzogranite in the study area.

	Mineral composition	Characteristics	Content
Syenogranite	K-feldspar	xenomorphic and granular; mudding and light brown; perthite and microcline; grain size 0.2–1 mm	50%–55%
	Quartz	xenomorphic and granular; grain size 0.2–1 mm	25%–30%
	Plagioclase	subhedral and columnar; fine polysynthetic twin; An25; grain size 0.2–1 mm	15%–20%
	Biotite	idiomorphic and schistose; brown; schist diameter 0.2–1 mm	a small amount
	Accessory mineral	Magnetite, zircon, apatite	a small amount
Monzogranite	K-feldspar	xenomorphic and granular; mudding and light brown; perthite and microcline; grain size 0.2–1 mm	30%–35%
	Plagioclase	subhedral and columnar; fine polysynthetic twin; An25; grain size 0.2–1 mm	25%–30%
	Quartz	xenomorphic and granular; grain size 0.2–1 mm	20%–25%
	Biotite	idiomorphic and schistose; brown; schist diameter 0.2–1 mm	2%–3%
	Accessory mineral	magnetite, zircon, apatite	a small amount

southeast Jiamusi Terrain, Meng et al. (2008)proposed that the Paleo-Asian Ocean between Jiamusi Terrain and Khanka Terrain disappeared in 268 Ma, followed by collision between the two terrains. Zhou et al. (2012) studied the geochronology of the Hutou complex rocks and discovered that the early Paleozoic magma and metamorphic event recorded by Hutou complex rocks in Khanka Terrain were consistent with the age of the Mashan Group in the western Jiamusi Terrain. They thus argued that the Khanka Terrain and the adjacent Jiamusi Terrain had an obvious structural affinity and had the same geological evolution history (Yang et al., 2012). Many other studies have compared the geographic features of the Carboniferous, Permian and Triassic strata and fossils distributed in the Khanka Terrain and South China Plate (Kobayashi, 1997; Kobayashi 2003). It is suggested that the Khanka Terrain was an exotic terrane with a South China Plate affinity (Zhang, 1997; Zhang, 2004), and might have belonged to the northeast part of the South China Plate (Li et al., 2017a; Guo et al., 2017).

Many epithermal deposits (e.g., Jinchang, Naozhi and Ciweigou gold deposits) have been discovered in the region adjacent to the Xinchenggou area (Qi et al., 2005), which show similar geological features. For example, in the Jinchang gold deposit and Naozhi copper-gold deposit granitoids mainly consists of granite, granite porphyry, syenogranite and monzogranite, and the main altered minerals are pyrite, sericite, feldspar, chlorite, epidote and so on in these two deposits (Zhu et al., 2003; Li, 2021). Beresitization (pyrite - sericite - silicification) is closely related to epithermal hydrothermal mineralization, which belongs to direct prospecting indicator. Meanwhile, there are also good geophysical and geochemical anomaly characteristics and mineralogical alteration characteristics in the study area. Sericite, adularia, argillite, chlorite, pyrite and other alteration minerals are found in the fractures of the granite body in the study area (Figure 4). It shows that the study area has the potential to search for epithermal hydrothermal deposits.

Meng (2012) determined that the zircons U-Pb age of granodiorite-porphyry directly related to mineralization in Yanghuidongzi copper deposit in the northern part of the study area is 194.8 ± 1.9 Ma, which is close to the regional magmatic rock age and roughly indicates the metallogenic age of Yanghuidongzi copper deposit.

The main strata in the study area are the volcanic rocks of the Late Triassic Luoquanzhan Formation (T_3l), whose formation ages are 206–213 Ma (Zhao et al., 2013; Wei, 2021). The petrogeochemical characteristics indicate that the volcanic rocks in the study area are partial melting products of crust. The volcanic rocks of the Luoquanzhan Formation mark the regional tectonic transformation from the end of Xing`anling-Mongolian orogeny to the initial of Pacific plate subduction to the Eurasia plate (Zhao et al., 2013). The preconcentration of gold element occurs in primary magma which formed Luoquanzhan Formation and provided part of ore material to Jinchang Cu-Au deposit (Zhao et al., 2013).

The main magma emplacement ages of granodiorite and monzonite, which are closely related to mineralization of Jinchang Cu-Au deposit, are 213 ± 1 Ma and 204. 8 ± 1.1 Ma, respectively. The magma evolution spans the Late Triassic and Early Jurassic (223–200 Ma), and has experienced multiple stages of rapid decompression and cooling, constant temperature and constant pressure crystallization (Han et al., 2015). The age of intrusive rocks in the Jinchang deposit is 163–203 Ma (Mu et al., 2000; Men, 2008), while the metallogenic age is 190–210 Ma (Men, 2008). Similar to these deposits, the granitoids in the Xinchenggou area are petrographically mainly composed of Mesozoic syenogranite and monzogranite. The formation ages of syenogranite and monzogranite are 222–190 Ma (the peak value is about 201 Ma) and 234–191 Ma (the peak value is about 205 Ma) (Han et al., 2010), indicating that syenogranite was emplaced slightly later than monzogranite (Zhang, 2016).

The ore-forming potential of the Mesozoic syenogranite and monzogranite in the Xinchenggou area is demonstrated by soil geochemical data (Hao and Wang 2017). The results of soil data in the Xinchenggou area show noticeable anomalies of Au, Ag, Cu, Mo, Bi, Sb and Sn, which are assemblages of medium-low temperature ore-forming elements common in epithermal deposits (Figure 5). The metal anomaly is mainly located in the contact zone of these Mesozoic syenogranite and the Late Triassic Luoquanzhan Formation tuff. The good ore-forming potential in the Xinchenggou area is further verified by the geophysical surveys (Figure 6), which have shown that there are good induced polarization (IP) anomalies and high magnetic anomalies around these plutons (Wang, 2018).

3 Sampling and analytical methods

Four representative samples of syenogranite (HQ-1, HQ-2, HQ-3 and HQ-5) and three samples of monzogranite (JX1304, JX1305 and

TABLE 2 Analytical results of whole-rock major (%) and trace elements (ppm) for granites in the Xinchenggou area, NE China.

Sample no.	HQ-1	HQ-2	HQ-3	HQ-5	JX1304	JX1305	1,322
Rock name	Syenogranite	Syenogranite	Syenogranite	Syenogranite	Monzogranite	Monzogranite	Monzogranite
SiO_2	76.78	74.56	72.12	71.23	74.20	75.16	76.42
Al_2O_3	11.98	12.68	13.07	13.52	13.15	12.85	12.70
Fe_2O_3	1.18	1.37	1.27	0.99	0.30	0.25	0.20
FeO	0.88	1.68	1.68	2.82	1.72	1.40	1.11
Fe_2O_3/FeO	1.34	0.82	0.76	0.35	0.18	0.18	0.18
TFeO	1.94	2.91	2.82	3.71	2.02	1.65	1.30
$Mg^{\#}$	8.41	20.06	28.78	30.18	21.00	20.00	15.00
K_2O	4.67	3.50	3.40	3.23	4.17	4.23	4.80
MgO	0.10	0.41	0.64	0.90	0.26	0.17	0.11
MnO	0.02	0.04	0.03	0.08	0.04	0.04	0.02
Na_2O	3.42	3.36	3.01	3.07	3.85	3.86	3.59
P_2O_5	0.01	0.05	0.08	0.08	0.03	0.02	0.02
CaO	0.52	1.45	1.26	2.20	1.12	0.94	0.71
TiO_2	0.09	0.24	0.33	0.42	0.16	0.13	0.10
LOI	0.28	0.49	2.93	1.31	0.58	0.34	0.39
Total	99.94	99.83	99.82	99.85	99.72	99.45	100.16
K_2O+Na_2O	8.09	6.86	6.41	6.30	8.02	8.09	8.39
K_2O/Na_2O	1.37	1.04	1.13	1.05	1.08	1.10	1.34
δ	1.94	1.49	1.41	1.41	2.06	2.04	2.11
A/CNK	1.03	1.06	1.20	1.08	1.02	1.02	1.02
A/NK	1.60	1.63	1.80	1.16	1.21	1.17	1.14
DI	94.15	86.90	85.63	79.67	90.03	91.83	93.71
SI	0.98	3.98	6.40	8.17	2.52	1.72	1.12
R_1	2,761	2,886	2,944	2,826	2,568	2,622	2,661
R_2	297	427	437	553	394	365	331
Rb	167.00	145.00	120.00	132.00	89.40	114.00	161.00
Ba	120	468	465	526	780	951	712
Nb	10.20	7.07	8.56	10.40	10.40	7.90	4.90
Ta	1.65	0.91	1.18	1.26	0.40	0.30	0.20
K	38,751.06	29,042.55	28,212.77	26,802.13	34,602.13	35,100.00	39,829.79
Sr	17.2	98.6	120.00	156.00	194.50	107.50	59.40
Cr	6.65	7.85	14.20	26.50	—	—	—
Ga	16.1	17.1	16.4	17.3	21.20	18.80	16.60
P	61.13	218.31	349.30	349.30	130.99	87.32	87.32
Hf	4.85	4.42	6.12	7.41	8.70	5.80	5.80
Th	—	—	—	—	7.43	9.50	2.10
Zr	113	215	106	127	375.00	219.00	91.00
Ti	564	1,440	1980	2,520	960	780	600

(Continued on following page)

TABLE 2 (*Continued*) Analytical results of whole-rock major (%) and trace elements (ppm) for granites in the Xinchenggou area, NE China.

Sample no.	HQ-1	HQ-2	HQ-3	HQ-5	JX1304	JX1305	1,322
Rock name	Syenogranite	Syenogranite	Syenogranite	Syenogranite	Monzogranite	Monzogranite	Monzogranite
Nb/Ta	6.18	7.77	7.25	8.25	26.00	26.33	24.50
Rb/Nb	16.37	20.51	14.02	12.69	8.60	14.43	32.86
Rb/Sr	9.71	1.47	1.00	0.85	0.46	1.06	2.71
Rb/Ba	1.39	0.31	0.26	0.25	0.11	0.12	0.23
Sr/Y	0.38	4.86	7.50	4.14	7.15	3.29	2.38
La	20.70	19.00	14.50	34.80	26.20	49.00	20.20
Ce	40.00	32.30	28.20	71.10	57.60	93.50	38.20
Pr	4.71	3.59	3.49	9.20	6.13	9.88	4.30
Nd	14.20	11.90	12.30	33.40	24.10	37.30	16.50
Sm	3.27	2.77	2.72	7.89	5.13	6.93	3.37
Eu	0.17	0.47	0.49	1.17	1.29	0.71	0.47
Gd	4.22	2.54	2.43	6.74	4.41	5.78	3.26
Tb	0.87	0.44	0.42	1.10	0.70	0.93	0.57
Dy	6.54	3.04	2.63	6.68	4.26	5.38	3.58
Ho	1.46	0.63	0.57	1.31	0.87	1.13	0.78
Er	4.65	1.97	1.79	3.76	2.66	3.03	2.32
Tm	0.76	0.32	0.29	0.57	0.42	0.50	0.39
Yb	5.42	2.29	2.18	3.77	2.73	3.09	2.61
Lu	0.85	0.35	0.34	0.53	0.47	0.48	0.39
Y	45.20	20.30	16.00	37.70	27.20	32.70	25.00
∑REE	107.82	81.61	72.35	182.02	136.97	217.64	96.94
∑LREE	83.05	70.03	61.70	157.56	120.45	197.32	83.04
∑HREE	24.77	11.58	10.65	24.46	16.52	20.32	13.90
∑LREE/∑HREE	3.35	6.05	5.79	6.44	7.29	9.71	5.97
δEu	0.14	0.54	0.58	0.49	0.83	0.34	0.43
δCe	0.99	0.96	0.97	0.97	1.11	1.04	1.00
La_N/Yb_N	2.74	5.95	4.77	6.62	6.88	11.37	5.55
La_N/Sm_N	4.09	4.43	3.44	2.85	3.30	4.56	3.87
Gd_N/Yb_N	0.64	0.92	0.92	1.48	1.34	1.55	1.03

Note: A/CNK = $Al_2O_3/(CaO+Na_2O+K_2O)$ (mole fraction ratio), A/NK = $Al_2O_3/(Na_2O+K_2O)$ (mole fraction ratio), $Mg^{\#}$ = 100×MgO/(MgO+TFeO) (mole fraction ratio), δ = $[w(K_2O)+w(Na_2O)]^2/w(SiO_2)$-43], DI = Q+Or+Ab+Ne+Lc+Kp (CIPW calculating data), SI = 100×MgO/(MgO+Fe_2O_3+FeO+Na_2O+K_2O)(wt%), R_1 = 4Si-11(Na+K)-2(Fe+Ti), R_2 = 6Ca+2 Mg+Al. Data for samples JX1304, JX1305 and 1,322 are from Jing et al. (2015).

1,322) were collected in the field from outcrops in the study area (Figure 7; Table 1). The samples HQ-1, HQ-2, HQ-3 and HQ-5 were collected 2 km southwest of Xinchenggou Village (131°03′39″E, 43°59′46″N; 131°03′34″E, 43°59′48″N; 131°03′36″E, 43°59′54″N; 131°03′36″E, 44°00′01″N; Figure 3). The samples JX1304 and JX1305 were collected from Jinchanggou pluton (131°08′31″E, 44°59′58″N; 131°08′18″E, 44°58′30″N; Figure 1B). The samples 1,322 was collected from Tianqiaoling pluton (131°01′24″E, 44°40′44″N; Figure 1B).

Mineralogically, syenogranite mainly contains K-feldspar, quartz, plagioclase, and to a lesser extent biotite. Compared to syenogranite, monzogranite contains more plagioclase and more biotite, and less feldspar. Accessory minerals in these granites are similar and include zircon, apatite and magnetite. Most of the collected samples underwent hydrothermal alteration to some degree. The most predominant alteration types are sericite-chlorite ± clay alteration. The mineralogical and alteration features are common for the ore-related intrusions from porphyry systems (Zhong et al., 2018a; Zhong et al.,

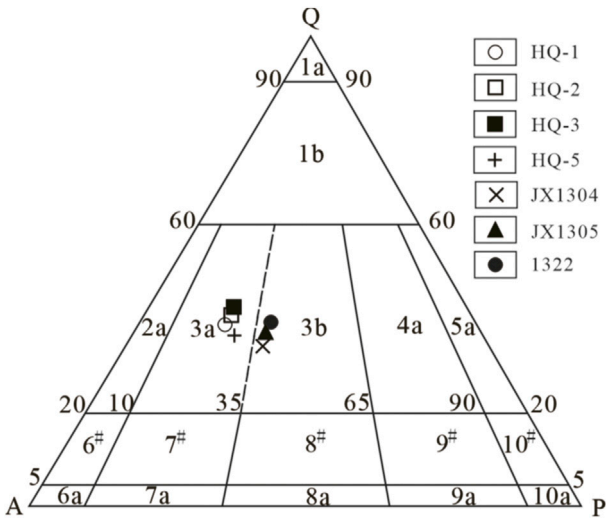

FIGURE 8
QAP diagram of granites in the Xinchenggou area, NE China (after Streckeisen, 1976). 1a- Quartzolite; 1b- Quartz-rich granitoid; 2a- Alkali-feldspar granite; 3a- Syenogranite; 3b- monzogranite; 4a- Granodiorite; 5a- Tonalite; 6#- Alkali feldspar quartz syenite; 7#- Quartz syenite; 8#- Quartz monzonite; 9#- Quartz monzodiorite; 10#- Quartz diorite; 6a- Alkali feldspar syenite; 7a- Syenite; 8a- Monzonite; 9a- Monzodiorite; 10a- Diorite/Gabbro/Anorthosite.

2018b; Qin et al., 2022). The least altered syenogranite samples were selected for whole-rock major and trace element analyses. However, since all the collected monzogranite in this study underwent strong sericitic alteration, geochemical analyses were not conducted for monogranite; rather, the whole-rock major and trace element data for monzogranite were compiled from the adjacent area (Jing et al., 2015).

The major elements and trace elements were analyzed in Yanjiao Central Laboratory of North China Non-ferrous Geological Exploration Bureau. The major elements were analyzed *via* the spectrophotometric method with 722 S visible spectrophotometer of Shanghai Spectral Instrument Co., Ltd. And GGX-6 atomic absorption spectrophotometer of Beijing Haiguang Instrument Factory; the analytical precision was above 5%; the trace elements and rare earth elements were analyzed with ICP-MS of PE Company; the analytical precision was above 10%. Meanwhile, to make the sample analysis results more representative, we also compiled the previously published data for monzogranite from the adjacent area (Jing et al., 2015). The sample analysis results are shown in Table 2.

4 Results

4.1 Major element characteristics

According to the major element analytical result, the SiO_2 content of granite in the study area is between 71.23% and 76.78%. Their aluminum is weakly supersaturated (Al_2O_3 = 11.98%–13.52%) MgO is 0.10%–0.90%, whereas the contents of TiO_2, Fe_2O_3 and P_2O_5 are low. In QAP diagram (Figure 8), the studied samples all plot into the syenogranite and monzogranite regions, which is consistent with the results based on petrography.

In the SiO_2-K_2O diagram (Figure 9A), all the samples are mainly located in the high-K calc-alkaline series region. K_2O+Na_2O ranges from 6.30% to 8.39% and the K_2O/Na_2O ratio is greater than 1.0. The aluminum saturation index (ACNK) of granites is 1.02~1.20, with six of seven samples characterized by ACNK<1.1. In A/CNK-A/NK diagram, the point of monzogranite is located in the weak peraluminous area, and the syenogranite is mainly located in the peraluminous area (Figure 9B). The differentiation index of granites (DI) is 79.67–94.15, indicating that the fractional crystallization effect of granite magma is relatively strong in this area. The solidification index of granites (SI) is 0.98–8.17, reflecting that the magmatic differentiation degree is high.

4.2 Rare earth element characteristics

Rare earth elements results (Figure 10A) show that the total REE contents are relatively low (∑REE = 72.35 × 10^{-6}~217.64 ×

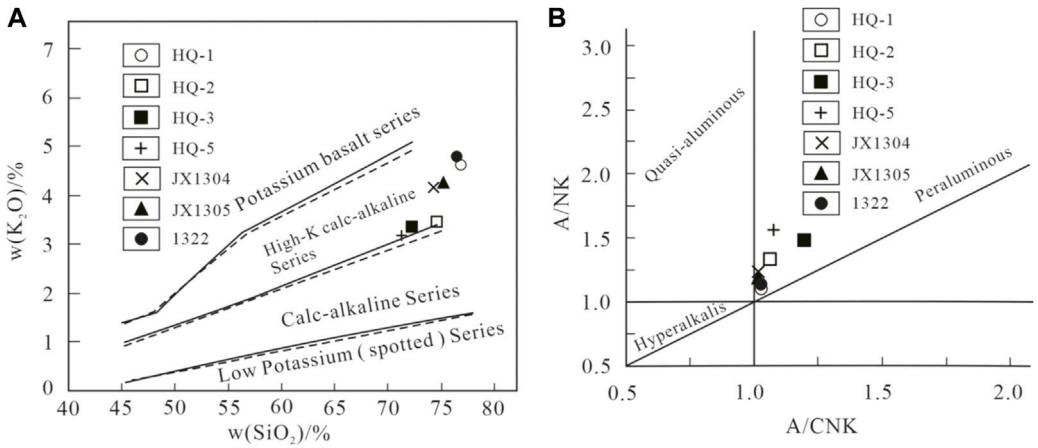

FIGURE 9
SiO_2-K_2O diagram **(A)** (real line after Peccerillo & Taylor, 1976; broken line after Middlemost, 1985) and A/CNK-A/NK diagram **(B)** (after Maniar & Piccoli, 1989) of granites in the Xinchenggou area, Dongning County.

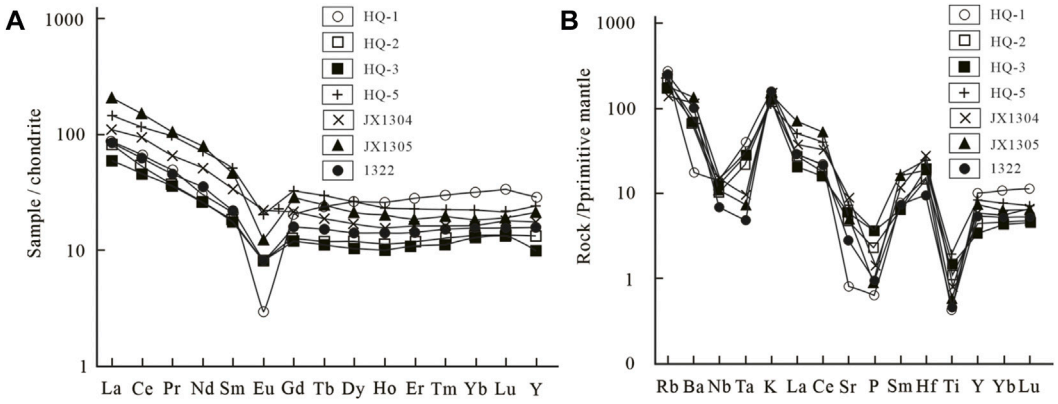

FIGURE 10
Chondrite-normalized REE patterns **(A)** and Primitive mantle-normalized spider diagrams **(B)** of granites in the Xinchenggou area, Dongning County (normalized data after Sun and McDonough, 1989).

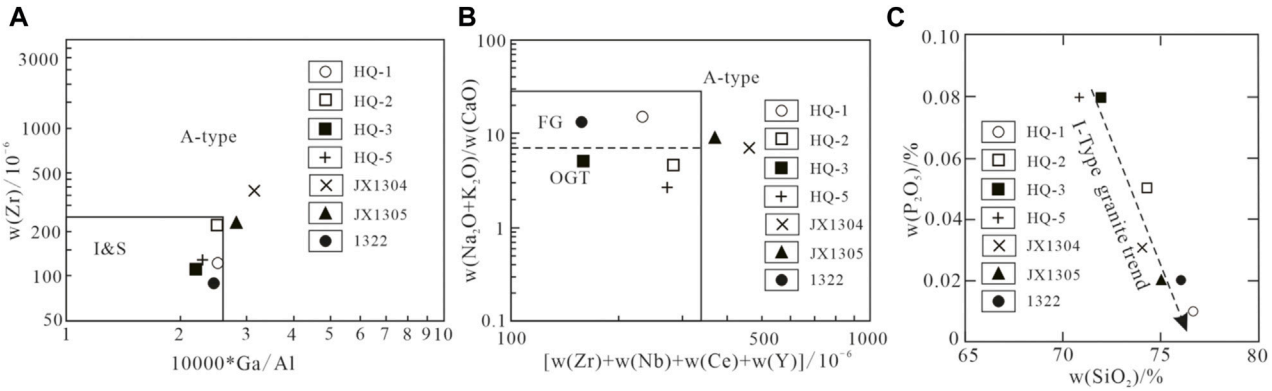

FIGURE 11
Discrimination diagrams for I-type granites in the Xinchenggou area, Dongning County. 10,000*Ga/Al versus Zr plots of A-type granites and I-, S-type granites (rectangular boxes) **(A)** (after Whalen et al., 1987); Zr+Nb+Ce+Y versus $(Na_2O+K_2O)/CaO$ plots of A-type granites and also fields for FG and OGT **(B)** (after Whalen et al., 1987); SiO_2 versus P_2O_5 harker diagram for I-type granites **(C)** (after Chappell and White, 1992; Chappell, 1999). Abbreviations: I&S-Field for I- and S-type granitoids; FG-Field for fractionated I- and S-type granitoids; OGT-Field for I-, S-, and M-type granitoids.

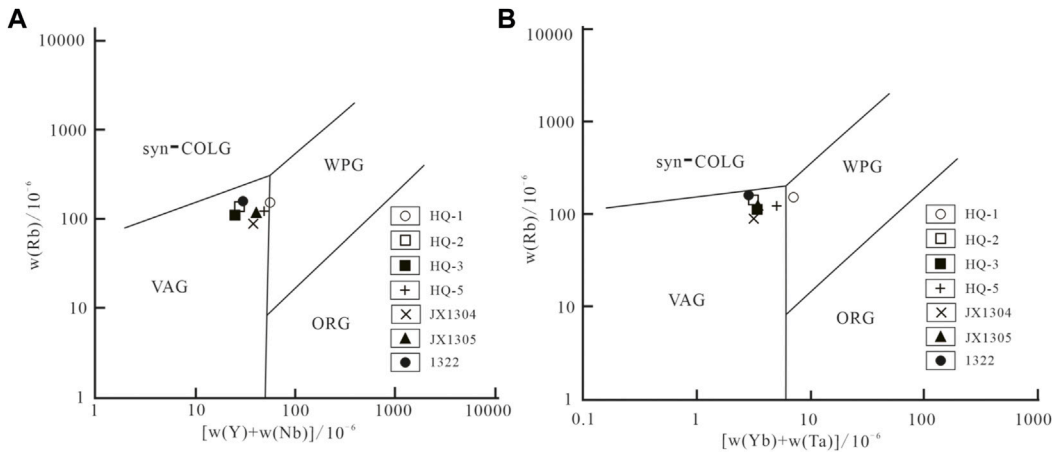

FIGURE 12
Nb-Y**(A)** and Rb-(Yb+Ta) **(B)** tectonic discrimination diagrams of granites in the Xinchenggou area, Dongning County (after Pearce et al., 1984). Abbreviations: syn-COLG = syn-collisional granite; VAG = volcanic arc granite; WPG = within-plate granite; ORG = ocean ridge granite.

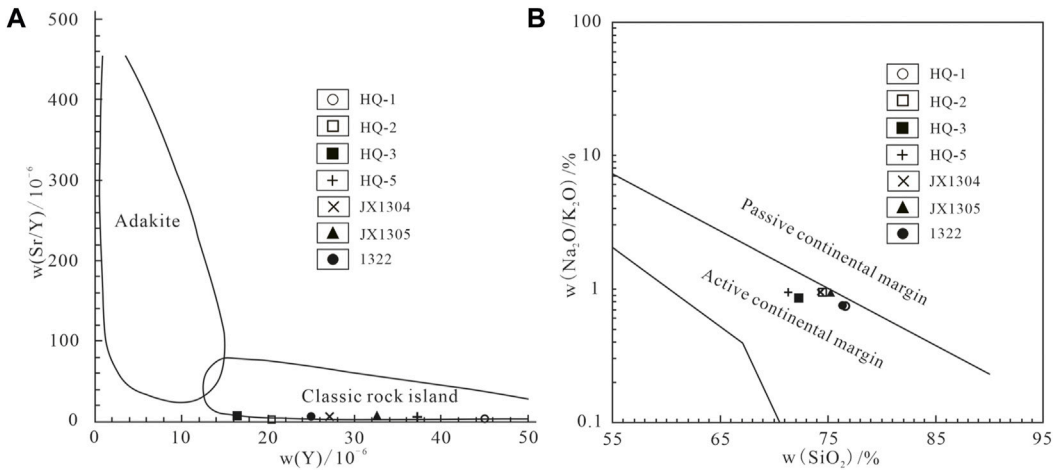

FIGURE 13
Sr/Y-Y **(A)** and Na_2O/K_2O-SiO_2 **(B)** tectonic discrimination diagrams of granites in the Xinchenggou area, Dongning County (A after Defant and Drummond, 1990; B after Roser and Korsch, 1986).

10^{-6} and ∑LREE/∑HREE is 3.35–9.71). LREE is comparatively enriched, whereas HREE is relatively depleted. La_N/Yb_N is 2.74–11.37 (the average value:6.27), indicating that light and heavy rare earth differentiation is strong. All intrusions are characterized by light rare earth element (LREE)-enriched patterns, as manifested in the chondrite-normalized rare earth element (REE) diagram. The Ce anomaly is not obvious, with δCe being 0.96–1.11. The Eu anomaly is noticeable with δEu characterized by 0.14–0.83.

4.3 Trace element characteristics

In the primitive mantle-normalized trace element diagram (Figure 10B), high-field-strength elements like Nb, Ta, P and Ti are comparatively depleted, and the depletion of P and Ti indicates that apatite and ilmenite present obvious fractional crystallization in the magmatic evolution process.

The negative anomalies of Nb, Ta, P and Ti, and the negative anomalies of large-ion lithophile element Sr, indicate the attribute of island arc magma (Li et al., 2019; Zhong et al., 2021a; Zhong et al., 2021b). It is suggested that the magma source area was contaminated and metasomatized by crustal materials or subduction residual oceanic crust fluids (Fitton et al., 1991).

The depletion of Nb and Ta reflects that the magma originates from crust or suffers from strong contamination of crust materials (Zhu et al., 2022). Large-ion lithophile elements like Rb, Ba, K and Hf are relatively enriched. The comparative enrichment of the strongly incompatible element Rb indicates that strong differentiation might happen during ascending of magmas (He et al., 2014).

Nb/Ta ratios range from 6.18 to 26.33, with an average value of 15.18, which are lower than the average value of 16.2 in the upper crust of eastern China and 18 in the primitive mantle (Sun and McDonough, 1989). These data indicate that the granitic magma source in the study area may derive from the upper mantle or lower crust, and a small amount of crustal material was involved during the formation process (Zhao et al., 1997; Hao and Wang 2017).

During magmatic evolution, although both the abundance of Nb and Ta increased, Ta increased more quickly than Nb. Therefore, the Nb/Ta ratio gradually decreased from early to late magmatic evolution (Chen et al., 2021). The Nb/Ta value of syenogranite in the study area is from 6.18 to 8.25, while the Nb/Ta value of monzogranite is from 24.5 to 26.33 (Jing et al., 2015), which also shows that the evolution stage of syenogranite in this area is later than that of monzogranite.

5 Discussion

5.1 Petrogenesis

Granitic rocks are commonly divided into I-, S- and A-types. A-type granites typically contain high-temperature anhydrous phases such as pyroxene and fayalite (e.g., King et al., 1997). The syenogranite and monozogranite that we studied contain minor biotite but lack pyroxene or fayalite. Furthermore, the syenogranite and monozogranite all belong to the high-K series and most have low Zr, Nb, and 10,000 × Ga/Al ratios, distinguishing them from A-type granites (Figure 11A; Whalen et al., 1987). Moreover, most of the samples we studied fall within the field of I- and S-type granites (Figure 11B). Chappell and White (1974) proposed that the boundary between S-type and I-type granites can be drawn at an A/CNK ratio of 1.1. Most of samples in this study are characterized by A/CNK ratio < 1.1, thus not consistent with that the studied samples are S-type rocks. Besides, S-type granites generally contain primary Al-rich minerals such as cordierite or muscovite, which were not observed from granites in the Xinchenggou area. Geochemically, S-type and I-type granites can also be distinguished by the relationship between SiO_2 and P_2O_5: P_2O_5 increases with SiO_2 for S-type granites whereas decreases for I-type granites. The observed negative relationship between SiO_2 and P_2O_5 thus indicates a petrogenesis of I-type granites (Figure 11C; Chappell and White, 1992; Chappell, 1999).

TABLE 3 Characteristics of deposits in the study area.

Deposit name	Surrounding rock	Ore-controlling structure/ orebody shape	Tectonic structure	Deposit type	Metallogenic material source	Intrusive age	Determination method and mineralization age
Jinchang gold deposit	Granodiorite, granite porphyry and granite	Breccia tube structure and ring, and radiating fracture; columnar and cryptomere	Intersection of Laoheishan—Suifen River Basin Fault and east-west fault zone in Jiamusi Terrain	Porphyritic type, explosion-breccia type, and epithermal type	Dioritic porphyrite and granite porphyry	163.3 Ma (Mu et al., 2000) 203 ± 3.6 Ma (Men, 2008)	Zircon U-Pb age 190-210 Ma (Men, 2008)
Wufeng gold deposit	Middle Jurassic Andesitic pyroclastic rocks	NE and NW fault; cryptomere and columnar	Mesozoic volcanic basin margin	Epithermal type	Pyroclastic rocks of Jingouling Formation, Upper Jurassic	K-Ar age 110~130 Ma (Feng, 1993)	Rb-Sr isochron age 144 ± 7 Ma (Zhao et al., 1996)
Wuxing gold deposit	Middle Jurassic coloradoite-rough subvolcanic rock	NW fault; network vein and disseminated	Mesozoic volcanic basin margin	Epithermal type	Subandesite of Upper Jurassic Jingouling Formation	K-Ar age 110~130 Ma (Feng, 1993)	Ar^{39}-Ar^{40} age 123 ± 7 Ma (Pang, 2009)
Naozhi copper & gold deposit	Granodiorite Plagiogranite	NW fault; irregular	Late Paleozoic fold basement uplift area in Mesozoic volcanic basin	Volcanic-subvolcanic hydrothermal gold deposit	Andesite –secondary andesite	K-Ar age and Rb-Sr isochron age 130~134 Ma (Huang, 1997)	Ar^{39}-Ar^{40} age 127.8 ± 0.2 Ma (Li et al., 2020)
Ciweigou gold deposit	Middle Jurassic Andesitic breccia tuff	Calderas and crevasses; nervation	Inner margin of Mesozoic volcanic basin	Epithermal type	Andesitic breccia lava	Zircon U-Pb 106.6 ± 2.1 Ma (Li, 2006) Ar^{39}-Ar^{40} plateau age 107.0 ± 0.6 Ma (Ji, 2007)	Ar^{39}-Ar^{40} age 105-102 Ma (Zhao et al., 2010)
Xiaoxinancha gold and copper deposit	Diorite and Qinglong Village metamorphic rocks	SN and EW fault control; stockwork and disseminated, and sulfide quartz vein type	Broken uplift region of Mesozoic volcanic basin margin	Porphyry-skarn-type	Medium-fine grained biotite monzogranite	Granitic complex zircon U-Pb age 112~104 Ma (Sun et al., 2008)	Zircon U-Pb age 123-102 Ma (Sun et al., 2007)
Tuanjiegou gold deposit	Yanshanian granodiorite porphyry and granite porphyry	Inner ring structure of volcanic and subvolcanic edifice; nervation, lenticular and lenticular	Intersection of Hegang Uplift and Wulaga Depression	Epithermal fissure filling type	Granite porphyry	Granitic porphyry zircon U-Pb age 107.0 ± 1.2 Ma (Han et al., 2012)	Zircon U-Pb age 102-100 Ma (Zhang et al., 2010a; Han et al., 2012)

Besides, syenogranite and monzogranite in the Xinchenggou area are characterized by relative enrichments of LREEs and depletion of HFSEs (e.g., Nb, Ta, and Ti), relatively flat HREE patterns, and negative Eu anomalies, consistent with the geochemical characteristics of subduction-related I-type magmas. In summary, these several lines of evidence suggest that the syenogranite and monzogranite in the Xinchenggou area are (slightly fractionated) I-type granites rather than A-type or S-type granites.

5.2 Tectonic setting

According to previous studies (Wang, 2018), the monzogranite in the epithermal Jinchang gold deposit near the study area has the geochemical characteristics of an active continental margin. In the tectonic discriminant diagram, these samples plot into volcanic arc granite region, which has the tectonic background related to ocean subduction and the characteristics of I-type granite. This is confirmed by the Nb-Y and Rb-(Yb + Ta) diagrams of Pearce et al. (1984) (Figure 12). In Figure 12, almost all syenogranite and monzogranite samples plot within volcanic arc granite region. In the Sr/Y-Y tectonic environment discrimination diagram, the intrusions in the study area are mainly located in the classic island arc granite region (Figure 13A). In the Na_2O/K_2O-SiO_2 diagram, two intrusions in the study area are mainly located in the active continental margin area (Figure 13B), indicating that two intrusions were formed in the island arc environment of the active continental margin.

Combined with previously published studies in the EXOB, we propose the following geodynamic models for the Xinchenggou granites and the related epithermal mineralization.

Many gold and copper (gold) deposits are discovered near the study area (Table 3; Figure 1), and the major deposit type is epithermal

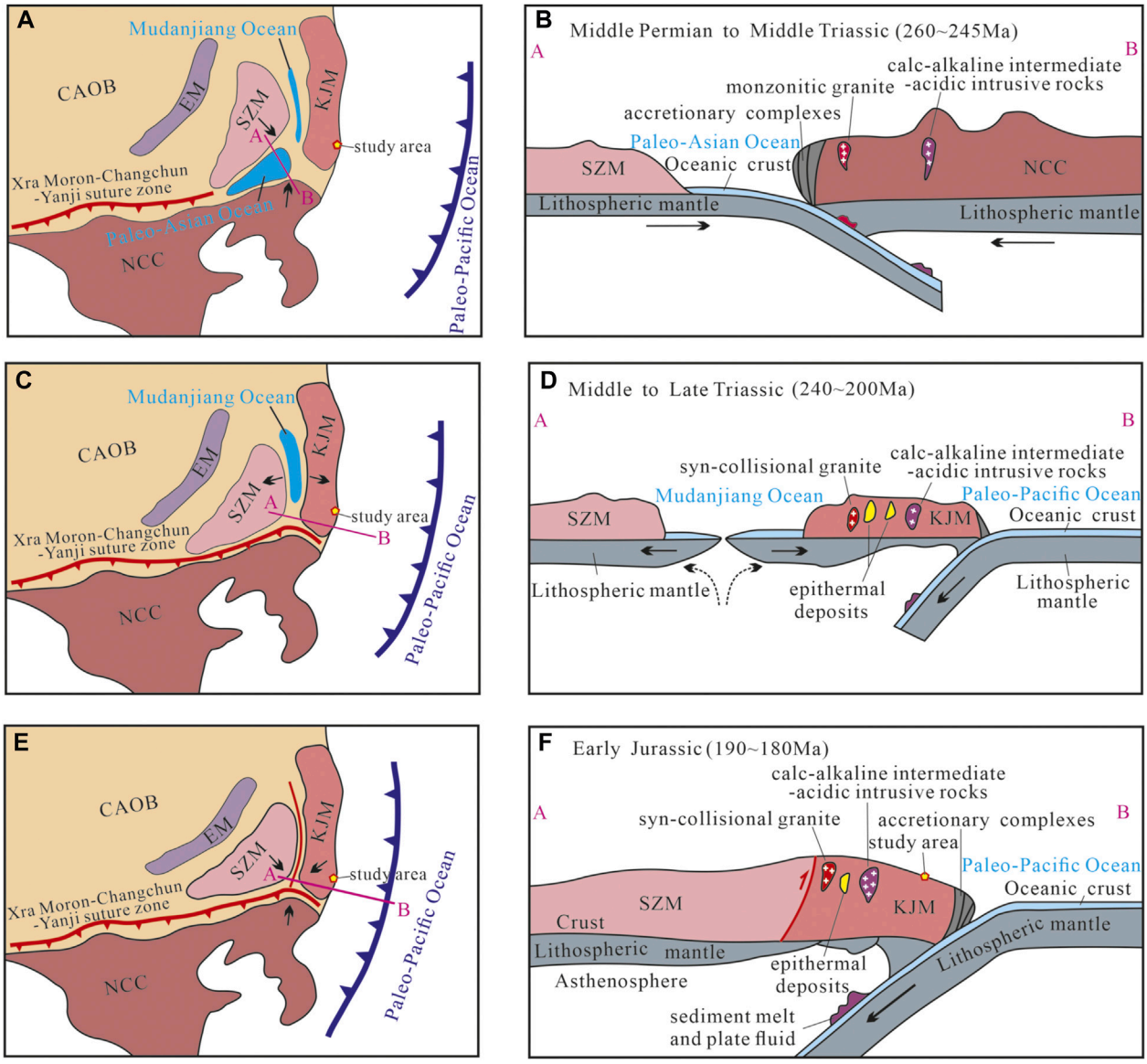

FIGURE 14
Tectonic scenarios under the Paleo-Asian Oceanic regime and the Paleo-Pacific regime during the Middle Permian to Early Jurassic (modified from Yang et al., 2017; 2018; Long et al., 2020; Wei, 2021). The scissor-like closure between the Songnen-Zhangguangcai Range block and North China Plate during the Middle-Permian to Middle-Triassic **(A,B)**; The subduction of the Pacific plate beneath the Eurasian plate began in Late Triassic **(C,D)**; The closure of Mudanjiang Ocean, formation of Syn-collision S-type granites and calc-alkaline I-type granites happened in Early Jurassic **(E,F)**.

-porphyry type; the mineralogenetic epoch mainly centers on 120–210 Ma, mainly mid-late Yanshanian period. This period is the important Cu metallogenic epoch (110–200 Ma) in Northeast China region, including one of the four age intervals of Mesozoic epithermal Au mineralization in Eastern China (144–135 Ma) (Lu et al., 2016). The weighted average age of zircon in dioritic porphyry and granite porphyry closely related to mineralization in the Jinchang gold deposit near the study area is 203 Ma, and the metallogenic time is speculated to 190–210 Ma (Men, 2008), it is Late Triassic-Early Jurassic.

During the Mesozoic, the Pacific Plate subducted beneath the Eurasian continental plate, forming a large-scale continental margin plate tectonic-magmatic metallogenic belt. Mesozoic epithermal gold deposits near the study area, such as Tuanjiegou gold deposit, Jinchang copper and gold deposit, formed in this tectonic-magmatic metallogenic belt of this tectonic background (Wan, 2013; Wu, 2018).

Located in Jilin-Heilongjiang provinces metallogenic belt in the east of Central Asian Orogenic Belt, the study area is in the superimposition and transition region of the E-W-trending Paleozoic Paleo-Asian Ocean Metallogenic Domain and the Mesozoic-Cenozoic Coastal Pacific Metallogenic Domain of NNE-orientated structure (Liu et al., 2004). The geological evolution of this area is complex and the minerogenetic condition is superior. Magmatic activities in the area are frequent, mainly dominated by the magmatism of the Mesozoic. A relatively favorable geological environment is provided for the mineralization of endogenous metal. Volcanic edifice and fault structure are developed, and channels and space are provided for ore-forming fluid migration and ore storage.

Generally speaking, the granites in study area have the transitional characteristics of I- and S-type granites, and the formation might be related to the tectonic environment of volcanic arc and tectonic event of syn-collision (Zhang, 2012). The magma generation type is transitional crustal syntectic type, and the syntectic type magma often appears in the active continental margin zone (Xu et al., 1983). The high Sr/Y granitoids of 251–245 Ma were found in the Solonker-Xar Moron River area on the southern margin of the Central Asian Orogenic Belt (Li et al., 2017b), and the adakitic granites were found in the central part of Jilin Province (Wang et al., 2015b). The geochronology, petrology and geochemistry of granitic rocks in the eastern segment of the Central Asian Orogenic Belt indicate that the collision between the North China Craton and the Khanka-Jiamusi Massif occurred during the Late-Permian to Early-Triassic along with the closure of the Paleo-Asian Ocean (Yang et al., 2018). A scissor-like closure of the Paleo-Asian Ocean from west to east between the Songnen-Zhangguangcai Range block and North China Plate took place during the Middle-Permian to Middle-Triassic (Figures 14A, B) (Wang et al., 2015a; b). Continental collision happened between the Songnen-Zhangguangcai Range block and North China Craton (Qi et al., 2005), forming the syn-collisional S granite. The collision and extrusion led to strong stacking and thickening of continental crust and lithosphere in the northeast. After extrusion and proliferation, extension-thinning was started.

At present, the timing of the subduction of the Pacific plate beneath the Eurasian plate is widely debated. Most researchers believe that the subduction of the Pacific plate beneath the Eurasian plate began during or before the Late Triassic (Isozaki et al., 2010; Wu et al., 2011; Li et al., 2012; Wilde Simon, 2015; Han et al., 2020; Liang et al., 2021). However, a few scholars believe that the subduction began in the Early Jurassic (Zhou et al., 2006; Xu et al., 2013b; Wang et al., 2015). Through deep analysis, this paper suggests that the subduction time is Late Triassic (Figures 14C, D). Due to this subduction, the Mudanjiang Ocean between the Songnen-Zhangguangcai Range blocks and the Khanka-Jiamusi block split anew in the Middle-Late Triassic (Xu et al., 2012). The 217–201 Ma of A-type volcanic rocks are developed in Yanbian-Dongning area (Wang et al., 2015a), and bimodal association of volcanic rocks are present in the region. The opening of NEE-NE trending Mesozoic-Cenozoic basin group (Yang et al., 2015; Yang et al., 2018), and the emplacement time of the Changchun-Yanji suture zone is 240–220 Ma (Cao et al., 2020), indicating that the Yanbian-Dongning area in the Late-Triassic was a back-arc extensional tectonic environment after the closure of the Paleo-Asian Ocean (Wang et al., 2015a). Meanwhile, as affected by post-orogenic extension, a large number of magmatic-hydrothermal metallogenic systems were developed, causing the formation of epithermal deposits (Qi et al., 2005; Zhang et al., 2008), such as the Jinchang gold deposit (Figures 14C, D).

In the Early Jurassic, the onset of subduction of the Paleo-Pacific Plate beneath the Eurasia Plate (Jing et al., 2015) led to the closure of the Mudanjiang Ocean between the Songnen-Zhangguangcai Range block and the Khanka-Jiamusi block. Early Jurassic calc-alkaline volcanic rocks in the eastern margin of Jilin-Heilongjiang provinces (Xu et al., 2013a; Wang Z. H. et al., 2017), the 205–160 Ma of calc-alkaline intrusive rocks (Yang et al., 2018), the low temperature dynamo metamorphism (193 Ma of biotite Ar-Ar age) of Huangsong Group in the eastern margin of Songnen-Zhangguangcai Range (Yu et al., 2015), and the Heilongjiang Complex with a metamorphic age of 175–186 Ma were all the products of the subduction of the Paleo-Pacific plate under Eurasia (Zhou et al., 2009; Wang Z. W. et al., 2017; Yang et al., 2018). Due to multiple tectonic compression, syn-collision S-type granites and calc-alkaline I-type granites were formed (Figures 14E, F) (Yang et al., 2017; Yang et al., 2018).

The Rb-Sr age of biotite in quartz diorite of Taiping Mountain near the study area is 250 Ma (HBGRM, 1979) the K-Ar age of biotite in granitic pluton of Taiping Mountain is 221.5 Ma (HBGRM, 1986); the weighted average age of zircon in granite porphyry of Jinchang gold deposit is 203 Ma (Men, 2008). Moreover, the intrusive rock near the study area can be divided into three invasion stages including Late Variscan, Early Indosinian and Late Indosinian. Some rocks also have the characteristics of S-type granite (HBGRM, 1986), showing that the granite in this area is characterized by multiple phases, multiple stages and compound origin.

6 Conclusion

1) The granites in the Xinchenggou area petrographically consist of syenogranite and monzogranite, which shows potential for epithermal-type for Au, Ag and Cu deposits.
2) Both syenogranite and monzogranite are high-K calc-alkaline and peraluminous, which belong to slightly fractionated I-type granites. The crust-mantle mixing effect of monzogranite is strong, while the crust-mantle mixing effect of syenogranite is relatively weak.
3) Syenogranite, monzogranite and epithermal deposits were emplaced in continental arc settings, which was related to the multiple-stage subduction of the Paleo-Pacific Plate beneath the Eurasian Plate during the Late Triassic to Early Jurassic.

Data availability statement

The original contributions presented in the study are included in the article/Supplementary Material, further inquiries can be directed to the corresponding authors.

Author contributions

YH: Investigation, Conceptualization, Formal analysis, Writing—original draft. LG: Writing—review and editing. YF: Writing—review and editing. Funding acquisition. HZ: Investigation. IS: Writing—review and editing. SL: Supervision, Writing—review and editing. JZ: Writing—review and editing.

Funding

The study is supported by the Geological Exploration Projects from Department of Natural Resources of Shandong Province (201558; 202055).

Conflict of interest

The authors declare that the research was conducted in the absence of any commercial or financial relationships that could be construed as a potential conflict of interest.

Publisher's note

References

Cao, J. L., Zhou, J. B., and Li, L. (2020). The tectonic evolution of the changchun-yanji suture zone: Constraints of zircon u-pb ages of the yantongshan accretionary complex (NE China). *J. Asian Earth Sci.* 194, 104110–104118. doi:10.1016/j.jseaes.2019.104110

Chappell, B. W. (1999). Aluminium saturation in I- and S-type granites and the characterization of fractionated haplogranites. *Lithos* 46, 535–551. doi:10.1016/s0024-4937(98)00086-3

Chappell, B. W., and White, A. J. R. (1992). I- and S-type granites in the lachlan fold belt. *Trans. R. Soc. Edinb. Earth Sci.* 83, 1–26. doi:10.1017/s0263593300007720

Chappell, B. W., and White, A. J. R. (1974). Two contrasting granite types. *Pac. Geol.* 8, 173174.

Chen, W., Zhang, G. L., Ruan, M. F., Wang, S., and Xiong, X. L. (2021). Genesis of intermediate and silicic arc magmas constrained by Nb/Ta fractionation. *J. Geophys. Res. Solid Earth* 126 (3), e2020JB020708. doi:10.1029/2020jb020708

Defant, M. J., and Drummond, M. S. (1990). Derivation of some modern arc magmas by melting of young subducted lithosphere. *Nature* 347 (6294), 662–665. doi:10.1038/347662a0

Deng, C., Li, C., Rong, Y., Chen, D., Zhou, T., Wang, X., et al. (2021). Different metal sources in the evolution of an epithermal ore system: Evidence from mercury isotopes associated with the Erdaokan epithermal Ag-Pb-Zn deposit, NE China. *Gondwana Res.* 95, 1–9. doi:10.1016/j.gr.2021.03.010

Feng, S. Z. (1993). Geological characteristics and metallogenic model of gold deposits in Wuxingshan- Wufeng, Jilin province. *Jilin Yejin* 1 (4), 2–5.

Fitton, J. G., James, D., and Leeman, W. P. (1991). Basic magmatism associated with late Cenozoic extension in the Western United States: Compositional variations in space and time. *J. Geophys. Res. Solid earth* 96 (8), 13693–13711. doi:10.1029/91jb00372

Gao, R., Xue, C., Lü, X., Zhao, X., Yang, Y., and Li, C. (2017). Genesis of the Zhengguang gold deposit in the Duobaoshan ore field, Heilongjiang Province, NE China: Constraints from geology, geochronology and S-Pb isotopic compositions. *Ore Geol. Rev.* 84, 202–217. doi:10.1016/j.oregeorev.2016.12.031

Ge, W. C., Wu, F. Y., Zhou, C. Y., and Zhang, J. H. (2007). Mineralization ages and geodynamic implications of porphyry Cu-Mo deposits in the east of Xingmeng orogenic belt. *Chin. Sci. Bull.* 52, 2407–2417. doi:10.1360/csb2007-52-20-2407

Guo, R. H., Li, S. Z., Suo, Y. H., Wang, Q., Zhao, S. J., Wang, Y. N., et al. (2017). Indentation of North China block into greater south China block and indosinian orocline. *Earth Sci. Front.* 24 (4), 171–184. doi:10.13745/j.esf.yx.2017-3-2

Han, Z. Z., Zhao, H. L., Li, J. J., Leng, C. N., Lü, J., and Li, W. L. (2010). Early mesozoic granites and polymetallic mineralization in southeastern yichun area, xiao hinggan mountains. *Geol. China* 37 (1), 74–87. doi:10.3969/j.issn.1000-3657.2010.01.008

Han, S. J., Sun, J. G., Zhang, Y., Xing, S. W., and Bai, L. A. (2012). Diagenetic and metallogenic mechanism of tuanjie gold deposit in the northern foothills of the lesser hinggan mountains: Constraints from zircon U-Pb chronology and Lu-Hf isotopes. *Mineral. Deposits* 31, 735–736.

Han, J. L., Wang, Q. H., Sun, J. G., Men, L. J., Chai, P., Zhao, K. Q., et al. (2015). Zircon U-Pb dating and magmatic evolution history tracing of Late Triassic-Early Jurassic granitic complex in Jinchang Cu-Au deposit area, eastern Heilongjiang. *Glob. Geol.* 34 (4), 938–950.

Han, W., Zhou, J. B., Wilde, S. A., and Long, Li (2020). LA-ICPMS zircon U-Pb dating of the Heilongjiang complex in the luobei area: New constraints for the late palaeozoic mesozoic tectonic evolution of Jiamusi block, NE China. *Geol. J.* 55 (3), 1644–1669. doi:10.1002/gj.3443

Hao, Y., and Wang, S. L. (2017). Geochemical characteristics and metallogenic potential of the subvolcanic rocks in Xieli area, Inner Mongolia. *Mineral. Explor.* 8 (5), 832–842.

HBGRM (Heilongjiang Bureau of Geology and Mineral Resources) (1979). *1: 200000 regional geological survey report (geological map of muling town and dongning county)*. Beijing: Geological Publishing House.

HBGRM (Heilongjiang Bureau of Geology and Mineral Resources) (1986). *1: 50000 regional geological survey report (geological map of dongning county, naozhigou and daduchuan)*. Beijing: Geological Publishing House.

He, H. H., Wang, D. H., Su, X. Y., Zhang, Y. J., Wang, G. R., Li, J. K., et al. (2014). Geochemical characteristics and ore potential of rare metal elements of the Qitianlin batholith in South Hunan, China. *Geotect. Metallogenia* 38 (2), 366–374.

Huang, G. C. (1997). Discussion on genetic relation between the Naozhi gold deposit and the Mesozoic volcanic rock series in Naozhi, Jilin province. *Mineral Resour. Geol.* 11 (1), 32–38.

Isozaki, Y., Aoki, K., Nakama, T., and Yanai, S. (2010). New insight into a subduction-related orogen: A reappraisal of the geotectonic framework and evolution of the Japanese islands. *Gondwana Res.* 18 (1), 82–105. doi:10.1016/j.gr.2010.02.015

Ji, W. Q. (2007). *Chronology and geochemistry of late mesozoic volcanic rocks in eastern Jilin and Heilongjiang provinces*. Changchun: Jilin University.

Jiang, B., Wang, D., Chen, Y., Zhang, T., Pu, X., Ma, W., et al. (2022). Classification, metallogenesis and exploration of silver deposits in Daxing'anling of Inner Mongolia and its adjacent areas. *China Geol.* 5, 1–19. doi:10.31035/cg2022005

Jing, H. X., Sun, D. Y., Gou, J., Wu, P. F., Wang, T. H., Guo, H. Y., et al. (2015). Chronology, geochemistry and Hf isotope of granite from southern Xingkai Block. *Earth Sci.* 40 (6), 982–994. doi:10.3799/dqkx.2015.082

King, P. L., White, A. J. R., Chappell, B. W., and Allen, C. (1997). Characterization and origin of aluminous A-type granites from the lachlan fold belt, southeastern Australia. *J. Petrology* 36, 371–391. doi:10.1093/petroj/38.3.371

Kobayashi, F. (2003). Palaeogeographic constraints on the tectonic evolution of the maizuru terrane of southwest Japan to the eastern continental margin of south China during the permian and triassic. *Palaeogeogr. Palaeoclimatol. Palaeoecol.* 195 (3-4), 299–317. doi:10.1016/s0031-0182(03)00363-8

Kobayashi, F. (1997). "Middle Permian biogeography based on fusulinacean faunas,". *Late paleozoic foraminifera: Their biostratigraphy, evolution, and paleoecology; and the mid-carboniferous boundary*. Editors C. A. Ross, J. R. P. Ross, and P. L. Brenckle (Cushman Foundation for Foraminiferal Research, Special publication), 36, 17–20.

Lan, H. Y., Li, S. Z., Guo, L. L., Li, X. Y., Liu, Y. J., Liu, B., et al. (2022). Mesozoic deformation of the nadanhada terrane (NE China) and its implications on the subduction of the Paleo-Pacific plate. *J. Asian Earth Sci.* 232, 105166–105180. doi:10.1016/j.jseaes.2022.105166

Li, C. W. (2006). in *Graduate school of the Chinese Academy of Sciences* (Guangzhou: Guangzhou Institute of Geochemistry), 5–98.*Petrogenesis and geological implications of the late Mesozoic volcanic rocks in southeastern Jilin province, northeastern China*

Li, X. P. (2021). *Study on metallogenesis of Naozhi copper-gold deposit, Yanbian area*. Changchun: Jilin University.

Li, S. Z., Santosh, M., Zhao, G. C., Zhang, G. W., and Jin, C. (2012). Intracontinental deformation in a frontier of super-convergence: A perspective on the tectonic milieu of the South China block. *J. Asian Earth Sci.* 49, 313–329. doi:10.1016/j.jseaes.2011.07.026

Li, S., Chung, S. L., Wilde, S. A., Jahn, B. M., Xiao, W. J., Wang, T., et al. (2017a). Early-middle triassic high Sr/Y granitoids in the southern central asian orogenic belt: Implications for ocean closure in accretionary orogens. *J. Geophys. Res. Solid Earth* 122 (6), 2291–2309. doi:10.1002/2017JB014006

Li, S., Jahn, B. M., Zhao, S. J., Dai, L. M., Li, X. Y., Suo, Y. H., et al. (2017b). Triassic southeastward subduction of North China Block to South China Block: Insights from new geological, geophysical and geochemical data. *Earth-Sci. Rev.* 166, 270–285. doi:10.1016/j.earscirev.2017.01.009

Li, H. L., Li, G. M., Liu, H., Huang, H. X., Cao, H. W., and Dai, Z. W. (2019). Petrogenesis of paleocene granite porphyry of daruo area in western lhasa block, tibet: Constraints from geochemistry, zircon U-Pb chronology and Sr-Nd-Pb-Hf isotopes. *Earth Sci.* 44 (7), 2275–2294.

Li, X. P., Sun, J. G., Liu, Y., Wang, Q. H., Ren, Z. N., and Gu, X. L. (2020). Zircon U-Pb chronology, geochemistry and geological implications of Mesozoic volcanic rocks from Naozhi copper-gold mining area. *Yanbian. Glob. Geol.* 39 (3), 528–543. (in Chinese). doi:10.3969/j.issn.1004-5589.2020.03.003

Liang, Y., Zheng, H., Li, H., Algeo, T. J., and Sun, X. M. (2021). Late paleozoic–mesozoic subduction and accretion of the Paleo-Pacific plate: Insights from ophiolitic rocks in the wandashan accretionary complex, NE China. *Geosci. Front.* 12 (6), 101242–101262. doi:10.1016/j.gsf.2021.101242

Liu, J. M., Zhang, R., and Zhang, Q. Z. (2004). The regional metallogeny of Da hinggan ling, China. *Earth Sci. Front.* 11 (1), 269–277. doi:10.3321/j.issn:1005-2321.2004.01.024

Liu, Y. J., Li, W. M., Ma, Y. F., Feng, Z. Q., Guan, Q. B., Li, S. Z., et al. (2021). An orocline in the eastern central asian orogenic belt. *Earth-Sci. Rev.* 221, 103808. doi:10.1016/j.earscirev.2021.103808

Long, X. Y., Xu, W. L., Guo, P., Sun, C. Y., and Luan, J. P. (2020). Opening and closure history of the Mudanjiang Ocean in the eastern central asian orogenic belt: Geochronological and geochemical constraints from early mesozoic intrusive rocks. *Gondwana Res.* 84, 111–130. doi:10.1016/j.gr.2020.03.003

Lu, Y. M., Suo, C. X., Zhuan, S. P., and Yin, M. (2016). Geochemistry and metallogenic potentiality of Early Cretaceous intrusive rocks in Ar Horqin area, Inner Mongolia. *Geophys. Geochem. Explor.* 40 (5), 885–892. doi:10.11720/wtyht.2016.5.07

Maniar, P. D., and Piccoli, P. M. (1989). Tectonic discrimination of granitoids. *Geol. Soc. Am. Bull.* 101 (5), 635–643. doi:10.1130/0016-7606(1989)101<0635:tdog>2.3.co;2

Men, L. J. (2008). *Geological, geochemical characteristics and metallogenic model of Jinchang super-large gold deposit, Dongning, Heilongjiang Province*. Master Degree Thesis. Changchun: Jilin University.

Meng, E., Xu, W. L., Yang, D. B., Pei, F. P., Yu, Y., and Zhang, X. Z. (2008). Permian volcanisms in eastern and southeastern margins of the Jiamusi Massif, northeastern China: Zircon U-Pb chronology, geochemistry and its tectonic implications. *Chin. Sci. Bull.* 53 (8), 1231–1245. doi:10.1007/s11434-008-0164-1

Meng, Z. X. (2012). *Genesis of the Yanghuidongzi copper deposit in dongning county, Heilongjiang province*. Changchun: Jilin University.

Middlemost, E. A. (1985). *Magmas and magmatic rocks: An introduction to igneous petrology*. London: Longman, 1–266.

Mu, T., Liu, G. G., and Xu, K. C. (2000). The geological-geochemical characteristics and ore Genesis of Jinchang gold deposit in Heilongjiang. *Gold Geol.* 6 (3), 57–64.

Ni, P., Chi, Z., and Pan, J. Y. (2020). An integrated investigation of ore-forming fluid evolution in porphyry and epithermal deposits and their implication on exploration. *Earth Sci. Front.* 27 (2), 60–78. doi:10.13745/j.esf.sf.2020.3.12

Ouyang, H. G., Mao, J. W., Santosh, M., Zhou, J., Zhou, Z. H., Wu, Y., et al. (2013). Geodynamic setting of mesozoic magmatism in NE China and surrounding regions: Perspectives from spatio-temporal distribution patterns of ore deposits. *J. Asian Earth Sci.* 78, 222–236. doi:10.1016/j.jseaes.2013.07.011

Pang, W. (2009). *Metallogenic model pf epithermal and low-sulfidation gold deposit, Yanbian area*. Changchun: Jilin University.

Pearce, J. A., Harris, N. B., and Tindle, A. G. (1984). Trace element discrimination diagrams for the tectonic interpretation of granitic rocks. *J. Pet.* 25 (4), 956–983. doi:10.1093/petrology/25.4.956

Peccerillo, A., and Taylor, S. R. (1976). Geochemistry of Eocene calc-alkaline volcanic rocks from the Kastamonu area, northern Turkey. *Contrib. Mineral. Petr.* 58 (1), 63–81. doi:10.1007/bf00384745

Qi, J. P., Chen, Y. J., and Franco, P. (2005). Geological characteristics and tectonic setting of the epithermal deposits in the northeast China. *J. Mineralogy Petrology* 25 (2), 47–59. doi:10.3969/j.issn.1001-6872.2005.02.009

Qin, J. H., Huang, F., Zhong, S. H., Wang, D. H., and Seltmann, R. (2022). Unraveling evolution histories of large hydrothermal systems via garnet U-Pb dating, sulfide trace element and isotopic analyses: A case study of shuikoushan polymetallic ore field, south China. *Ore Geol. Rev.* 149, 105063. doi:10.1016/j.oregeorev.2022.105063

Roser, B. P., and Korsch, R. J. (1986). Determination of tectonic setting of sandstone-mudstone suites using SiO_2 content and K_2O/Na_2O ratio. *J. Geol.* 94, 635–650. doi:10.1086/629071

Streckeisen, A. (1976). Classification of the common igneous rocks by means of their chemical composition: A provisional attempt. *Neues Jahrb. für Mineral. Monatsh.* 12 (1), 1–15.

Sun, J. G., Zhao, J. K., Chen, J. Q., Nagao, K., Sumino, H., Shen, K., et al. (2007). Ore forming mechanism for the Xiaoxinancha Au rich Cu deposit in Yanbian, Jilin Province, China: Evidence from noble gas isotope geochemistry of fluid inclusions in minerals. *Sci. China (Series D)* 37 (12), 1588–1598. doi:10.1360/zd2007-37-12-1588

Sun, J. G., Chen, L., Zhao, J. K., Men, L. J., Pang, W., Chen, D., et al. (2008). SHRIMP U-Pb dating of zircons from Late Yanshanian granitic complex in Xiaoxinancha gold-rich copper orefield of Yanbian and its geological implications. *Mineral. Deposits* 27 (3), 319–328. doi:10.3969/j.issn.0258-7106.2008.03.003

Sun, S. S., and McDonough, W. F. (1989). Chemical and isotopic systematics of oceanic basalts: Implications for mantle composition and processes. *Geol. Soc. Lond. Spec. Publ.* 42 (1), 313–345. doi:10.1144/gsl.sp.1989.042.01.19

Tang, H. J., Deng, Z., Zhong, S. H., Meng, G. X., Wang, Z. L., Yuan, L. L., et al. (2023). Geochemistry and Sr–Nd–Hf–O isotopes of ore-bearing plutons from the Yundukala Au–Cu–Co deposit, East Junggar, Xinjiang, Northwest China: Implications for petrogenesis and tectonic setting. *Ore Geol. Rev.* 153, 105274. doi:10.1016/j.oregeorev.2022.105274

Wan, F. (2013). *Characteristics, genesis and prospecting criteria of the Mesozoic epithermal gold deposits in Yanbian area*. Changchun: Jilin University

Wang, H. Z., and Mo, X. X. (1995). An outline of the tectonic evolution of China. *Episodes* 18, 6–16. doi:10.18814/epiiugs/1995/v18i1.2/003

Wang, Y. W., Wang, J. B., Long, L. L., Zou, T., and Wang, L. J. (2012). Tectonic evolution stages of northern Xinjiang and tectonic types of porphyry-epithermal deposits. *Geol. China* 39 (3), 695–716. doi:10.1007/s11783-011-0280-z

Wang, F., Xu, W. L., Xu, Y. G., Gao, F. H., and Ge, W. C. (2015). Late triassic bimodal igneous rocks in eastern Heilongjiang province, NE China: Implications for the initiation of subduction of the Paleo-Pacific Plate beneath Eurasia. *J. Asian Earth Sci.* 97, 406–423. doi:10.1016/j.jseaes.2014.05.025

Wang, Z. J., Xu, W. L., Pei, F. P., Wang, Z. W., and Li, Y. (2015a). Geochronology and provenance of detrital zircons from late palaeozoic strata of central Jilin province, northeast China: Implications for the tectonic evolution of the eastern central asian orogenic belt. *Int. Geol. Rev.* 57 (2), 211–228. doi:10.1080/00206814.2014.1002118

Wang, Z. J., Xu, W. L., Pei, F. P., Wang, Z. W., Li, Y., and Cao, H. H. (2015b). Geochronology and geochemistry of middle Permian-Middle Triassic intrusive rocks from central-eastern Jilin Province, NE China: Constraints on the tectonic evolution of the eastern segment of the Paleo-Asian Ocean. *Lithos* 238, 13–25. doi:10.1016/j.lithos.2015.09.019

Wang, Y. B., Zeng, Q. D., Zhou, L. L., Chu, S. X., and Guo, Y. P. (2016a). The sources of ore-forming material in the low-sulfidation epithermal Wulaga gold deposit, NE China: Constraints from S, Pb isotopes and REE pattern. *Ore Geol. Rev.* 76, 140–151. doi:10.1016/j.oregeorev.2016.01.012

Wang, F., Xu, W. L., Ge, W. C., Yang, H., Pei, F. P., and Wu, W. (2016b). The offset distance of the Dunhua-Mishan Fault: Constraints from paleozoic-mesozoic magmatism within the songnen-zhangguangcai range, Jiamusi, and Khanka massifs. *Acta Pet. Sin.* 32 (4), 1129–1140.

Wang, Z. H., Ge, W. C., Yang, H., Bi, J. H., Ji, Z., Dong, Y., et al. (2017a). Petrogenesis and tectonic implications of Early Jurassic volcanic rocks of the Raohe accretionary complex, NE China. *J. Asian Earth Sci.* 134, 262–280. doi:10.1016/j.jseaes.2016.09.021

Wang, Z. W., Xu, W. L., Pei, F. P., Guo, P., Wang, F., and Li, Y. (2017b). Geochronology and geochemistry of early paleozoic igneous rocks from the zhangguangcai range, northeastern China: Constraints on tectonic evolution of the eastern central asian orogenic belt. *Lithosphere* 9 (5), 803–827. doi:10.1130/L639.1

Wang, R. L., Zeng, Q. D., Zhang, Z. C., Zhou, L. L., and Qin, K. Z. (2021). Extensive mineralization in the eastern segment of the Xingmeng orogenic belt, NE China: A regional view. *Ore Geol. Rev.* 135, 104204–104230. doi:10.1016/j.oregeorev.2021.104204

Wang, Z. G. (2018). *Mineralization and metallogenic prediction of Jinchang Cu-Au deposit in dongning, Heilongjiang province*. Changchun: Jilin University.

Wei, J. Y. (2021). *Petrogenesis and geodynamics of late triassic to early jurassic volcanic rocks in yanbian-dongning area*. Changchun: Jilin University.

Whalen, J. B., Currie, K. L., and Chappell, B. W. (1987). A-Type granites: Geochemical characteristics, discrimination and petrogenesis. *Contributions Mineralogy Petrology* 95, 407–419. doi:10.1007/bf00402202

Wilde Simon, A. (2015). Final amalgamation of the central asian orogenic belt in NE China: Paleo-Asian ocean closure versus Paleo-Pacific plate subduction - a review of the evidence. *Tectonophysics* 662, 345–362. doi:10.1016/j.tecto.2015.05.006

Wu, F. Y., Sun, D. Y., Ge, W. C., Zhang, Y. B., Grant, M. L., Wilder, S. A., et al. (2011). Geochronology of the phanerozoic granitoids in northeastern China. *J. Asian Earth Sci.* 41 (1), 1–30. doi:10.1016/j.jseaes.2010.11.014

Wu, M. (2018). *The type, metallogenic characteristics and regularity of gold deposits in the mid-eastern part of Heilongjiang Province*. Changchun: Jilin University.

Xiao, W. J., Windley, B. F., Hao, J., and Zhai, M. G. (2003). Accretion leading to collision and the permian solonker suture, inner Mongolia, China: Termination of the central asian orogenic belt. *Tectonics* 22 (6), 1–21. doi:10.1029/2002tc001484

Xu, K. Q., Hu, S. X., Sun, Z. M., Zhang, J. R., and Ye, J. (1983). On the genetic series of granites, as exemplified by the Mesozoic granite of South China. *Acta Geol. Sin.* 56, 107–118.

Xu, W. L., Wang, F., Meng, E., Gao, F. H., Pei, F. P., Yu, J. J., et al. (2012). Paleozoic-early mesozoic tectonic evolution in the eastern Heilongjiang province, NE China: Evidence from igneous rock association and U-Pb geochronology of detrital zircons. *J. Jilin Univ. (Earth Sci. Ed.* 42 (5), 1378–1389. doi:10.13278/j.cnki.jjuese.2012.05.024

Xu, W. L., Pei, F. P., Wang, F., Meng, E., Ji, W. Q., Yang, D. B., et al. (2013a). Spatial-temporal relationships of mesozoic volcanic rocks in NE China: Constraints on tectonic overprinting and transformations between multiple tectonic regimes. *J. Asian Earth Sci.* 74, 167–193. doi:10.1016/j.jseaes.2013.04.003

Xu, W. L., Wang, F., Pei, F. P., Meng, E., Tang, J., Xu, M. J., et al. (2013b). Mesozoic tectonic regimes and regional ore-forming background in NE China: Constraints from spatial and temporal variations of Mesozoic volcanic rock associations (in Chinese). *Acta Petrol. Sin.* 29 (2), 339–353.

Xu, W. L., Sun, C. Y., Tang, J., Luan, J. P., and Wang, F. (2019). Basement nature and tectonic evolution of the xing'an-Mongolian orogenic belt. *Earth Sci.* 44 (5), 1620–1646. doi:10.3799/dqkx.2019.036

Yang, H., Zhang, Y. L., Chen, H. J., and Ge, W. C. (2012). Zircon U-Pb ages of Khanka Lake granitic complex and its geological implication. *Glob. Geol.* 31 (4), 621–630. doi:10.3969/j.issn.1004-5589.2012.04.001

Yang, H., Ge, W. C., Zhao, G. C., Yu, J. J., and Zhang, Y. L. (2015). Early permian-late triassic granitic magmatism in the jiamusi-khanka Massif, eastern segment of the central asian orogenic belt and its implications. *Gondwana Res.* 27 (4), 1509–1533. doi:10.1016/j.gr.2014.01.011

Yang, D. G., Sun, D. Y., Gou, J., and Hou, X. G. (2017). U-Pb ages of zircons from Mesozoic intrusive rocks in the Yanbian area, Jilin Province, NE China: Transition of the Paleo-Asian oceanic regime to the circum-Pacific tectonic regime. *J. Asian Earth Sci.* 143, 171–190. doi:10.1016/j.jseaes.2017.04.019

Yang, D. G., Sun, D. Y., Hou, X. G., Mao, A. Q., Tang, Z. Y., and Qin, Z. (2018). Geochemistry and zircon Hf isotopes of the early mesozoic intrusive rocks in the South hunchun, yanbian area, northeast China: Petrogenesis and implications for crustal growth. *Int. Geol. Rev.* 60 (8), 1038–1060. doi:10.1080/00206814.2017.1365019

Yu, J. J., Xu, W. L., Gao, F. H., Wang, F., Liu, J. C., and Hao, W. L. (2015). Medium-pressure metamorphism of the Huangsong Group in the southeastern margin of the Xing'an-Mongolian Orogenic Belt, NE China and its tectonic implication: Evidence

from petrology, mineralogy and 40Ar/39Ar geochronology. *Acta Petrol. Sin.* 31 (9), 2477–2494.

Zeng, Q. D., Liu, J. M., Yu, C. M., Ye, J., and Liu, H. T. (2011). Metal deposits in the Da Hinggan Mountains, NE China:styles, characteristics, and exploration potential. *Int. Geol. Rev.* 53 (7), 846–878. doi:10.1080/00206810903211492

Zeng, Q. D., Liu, J. M., Chu, S. X., Wang, Y. B., Sun, Y., Duan, X. X., et al. (2012). Mesozoic molybdenum deposits in the east Xingmeng orogenic belt, northeast China: Characteristics and tectonic setting. *Int. Geol. Rev.* 54 (16), 1843–1869. doi:10.1080/00206814.2012.677498

Zeng, Q. D., Liu, J. M., Qin, K. Z., Fan, H. R., Chu, S. X., Wang, Y. B., et al. (2013). Types, characteristics, and time-space distribution of molybdenum deposits in China. *Int. Geol. Rev.* 55 (11), 1311–1358. doi:10.1080/00206814.2013.774195

Zhang, K. J. (1997). North and South China collision along the eastern and southern North China margins. *Tectonophysics* 270 (1-2), 145–156. doi:10.1016/s0040-1951(96)00208-9

Zhang, K. J. (2004). Granulite xenoliths from cenozoic basalts in SE China provide geochemical fingerprints to distinguish lower crust terranes from the North and South China tectonic blocks: Comment. *Lithos* 73 (1-2), 127–134. doi:10.1016/j.lithos.2003.10.005

Zhang, Q. (2012). Collision and granite: Collision is a tectonic event, not a tectonic environment. *Acta Petrologica Mineralogica* 31 (5), 745–749. doi:10.1007/s11783-011-0280-z

Zhang, Y. S. (2016). *Characteristics and genesis of magmatic rocks of laoheishan and Jinchang area, Heilongjiang province*. Beijing: China University of Geosciences. (in Chinese).

Zhang, Y., Lai, Y., Qing, M., Wang, Y. Z., and Xu, J. J. (2008). Ore-fluid geochemistry of the J0 orebody, Jinchang gold deposit, Heilongjiang Province, China. *Acta Pet. Sin.* 24 (5), 1131–1144.

Zhang, J., Chen, Y. R., Xie, T. Y., Li, F. Y., Yuan, Y. H., Zhao, J., et al. (2010a). A tentative discussion on the genesis, ore-controlling regularity and prospecting direction of the Tuanjiegou gold deposit. *Geol. China* 37 (6), 1710–1719.

Zhang, Z. C., Mao, J. W., Wang, Y. B., Pirajno, F., Liu, J. L., and Zhao, Z. D. (2010b). Geochemistry and geochronology of the volcanic rocks associated with the Dong'an adularia-sericite epithermal gold deposit, Lesser Hinggan Range, Heilongjiang province, NE China: Constraints on the metallogenesis. *Ore Geol. Rev.* 37 (3), 158–174. doi:10.1016/j.oregeorev.2010.03.001

Zhang, Y., Song, Q. H., Han, S. J., and Ding, J. H. (2022). Geochronology and geochemistry of the hekoulinchang Sn-Pb-Zn-Ag polymetallic deposit (73240 t) in Heilongjiang province, China. *China Geol.* 5 (1), 46–59. doi:10.1016/S2096-5192(22)00085-4

Zhao, C. J., Peng, Y. J., Dang, Z. X., Zhang, Y. P., and Zhu, Q. (1996). *Tectonic framework and crust evolution of eastern Jilin and Heilongjiang provinces: Shenyang*. China: Liaoning University Press.

Zhao, Y. M., Zhang, D. Q., and Sheng, J. F. (1997). *Metallogenic regularity and prospective evaluation of copper polymetallic deposits of Da Hinggan Mountains and its adjacent areas*. Beijing: Seismological Press.

Zhao, Y. J., Sun, J. G., Wang, Q. H., Men, L. J., Li, Y. X., Guo, J., et al. (2010). $^{40}Ar/^{39}Ar$ laser probe dating and discussion on metallogenic epoch of epithermal Au-Cu deposit in Yanbian area of Jilin. *Earth Sci. Front.* 17 (2), 156–169.

Zhao, Y. S., Yan, J. P., Yang, L. Q., Chen, Y. F., and Wang, J. R. (2013). Zircon U-Pb chronology and its significance for volcanic rocks from Jinchang Cu-Au deposit, Heilongjiang Province. *J. Mineralogy Petrology* 33 (2), 50–58. doi:10.19719/j.cnki.1001-6872.2013.02.008

Zhong, S. H., Seltmann, R., and Shen, P. (2017). Two different types of granitoids in the Suyunhe large porphyry Mo deposit, NW China and their genetic relationships with molybdenum mineralization. *Ore Geol. Rev.* 88, 116–139. doi:10.1016/j.oregeorev.2017.04.012

Zhong, S. H., Feng, C. Y., Seltmann, R., Dolgopolova, A., Andersen, J. C. Ø., Li, D. X., et al. (2018a). Sources of fluids and metals and evolution models of skarn deposits in the qimantagh metallogenic belt: A case study from the weibao deposit, east kunlun mountains, northern Tibetan plateau. *Ore Geol. Rev.* 93, 19–37. doi:10.1016/j.oregeorev.2017.12.013

Zhong, S. H., Feng, C. Y., Seltmann, R., Li, D. X., and Dai, Z. H. (2018b). Geochemical contrasts between late triassic ore-bearing and barren intrusions in the weibao Cu–Pb–Zn deposit, east kunlun mountains, NW China: Constraints from accessory minerals (zircon and apatite). *Miner. Deposita* 53 (6), 855–870. doi:10.1007/s00126-017-0787-8

Zhong, S. H., Li, S. Z., Feng, C. Y., Gao, Y. B., Qu, H. Q., Seltmann, R., et al. (2021a). Geochronology and geochemistry of mineralized and barren intrusive rocks in the yemaquan polymetallic skarn deposit, northern qinghai-tibet plateau: A zircon perspective. *Ore Geol. Rev.* 139, 104560. doi:10.1016/j.oregeorev.2021.104560

Zhong, S. H., Li, S. Z., Feng, C. Y., Liu, Y. J., Santosh, M., He, S. Y., et al. (2021b). Porphyry copper and skarn fertility of the northern Qinghai-Tibet Plateau collisional granitoids. *Earth-Science Rev.* 214, 103524–103622. doi:10.1016/j.earscirev.2021.103524

Zhou, J. B., and Wilde, S. A. (2013). The crustal accretion history and tectonic evolution of the NE China segment of the Central Asian Orogenic Belt. *Gondwana Res.* 23, 1365–1377. doi:10.1016/j.gr.2012.05.012

Zhou, X. M., Sun, T., Shen, W. Z., Shu, L. S., and Niu, Y. L. (2006). Petrogenesis of mesozoic granitoids and volcanic rocks in south China: A response to tectonic evolution. *Episodes* 29 (1), 26–33. doi:10.18814/epiiugs/2006/v29i1/004

Zhou, J. B., Wilde, S. A., Zhang, X. Z., Zhao, G. C., Zheng, C. Q., Wang, Y. J., et al. (2009). The onset of Pacific margin accretion in NE China: Evidence from the Heilongjiang high-pressure metamorphic belt. *Tectonophysics* 478, 230–246. doi:10.1016/j.tecto.2009.08.009

Zhou, J. B., Zeng, W. S., Cao, J. L., Han, J., and Guo, X. D. (2012). The tectonic framework and evolution of the NE China: From ~ 500 Ma to ~ 180 Ma. *J. Jilin Univ. (Earth Sci. Ed.* 42 (5), 1298–1316. doi:10.1007/s11783-011-0280-z

Zhu, C. W., Chen, J. R., Li, T. G., Cui, B., Jin, B. Y., and Wang, K. Q. (2003). Geology and ore genesis of Jinchang gold deposit, Heilongjiang province. *Mineral. Deposits* 22 (1), 56–64.

Zhu, D. Q., Tang, M. Y., Ding, Z. J., Zhu, H. B., Wang, W. X., Zhang, Y., et al. (2022). Petrogenesis and geodynamic setting of granite porphyry dike in saibagou gold deposit, northern margin of qaidam: Evidence from geochronology and geochemistry. *Geoscience* 36 (3), 898–910. doi:10.19657/j.geoscience.1000-8527.2021.05